This is to certify that the

thesis entitled

STEADY STATE INVERSE THERMAL ANALYSIS IN SUPERCOOLED ACCELERATOR CAVITIES

presented by

AHMAD AIZAZ

has been accepted towards fulfillment of the requirements for

MASTERS degree in MECHANICAL ENGINEERING

Major professor

Date 3/10/03

# STEADY STATE INVERSE THERMAL ANALYSIS IN SUPERCOOLED ACCELERATOR CAVITIES

BY

AHMAD AIZAZ

A THESIS

Submitted to
Michigan State University
In partial fulfillment of the requirements
for the degree of

MASTER OF SCIENCE

Department of Mechanical Engineering

2003

# ABSTRACT

# STEADY STATE INVERSE THERMAL ANALYSIS IN SUPERCOOLED ACCELERATOR CAVITIES

BY

AHMAD AIZAZ

A heat conduction problem in Super Conducting Radio Frequency (SRF) cavities has been studied. The wall thickness is 1-4mm niobium and a 'point heating' source on the inner surface of the evacuated niobium cavity is assumed. Liquid helium acts as a coolant on the outer surface of the cavity to make the niobium electrically super conducting below its critical temperature. Using finite difference techniques, a computer program has been developed to solve the direct steady-state heat conduction equation. To simulate the actual thermal diagnostic setup at the Cyclotron Laboratory as closely as possible, the geometry for this computer program is 3-dimensional with insulated thermal sensors installed on the outer surface of the cavity. The insulated enclosures have different thermal properties from those of the niobium.

The results obtained through the program are useful for understanding the maximum sensor spacing, which allows detection of a 1 degree temperature rise at the heated surface (inner side) of the cavity.

Code verification is done with results obtained through the exact solutions generated by COND3D, developed for Sandia National Laboratory, and through the Kokopelli Finite Element Method program developed for Los Alamos National Laboratory. The results are discussed in detail with suggestions for future research.

## ACKNOWLEDGEMENTS

I would like to take this opportunity to thank James Calthorp, Steve Bricker and Scott Hitchcock for their invaluable practical help in performing thermometric experiments at the National Superconducting Cyclotron Laboratory (NSCL), at Michigan State University (MSU). I would also like to thank Dr. Terry Grimm and Dr. Walter Hartung for many helpful discussions and explanations of the physics of thermometry in RF cavities.

My special thanks go to Dr. Robert L. McMasters whose patient guidance gave this work direction and purpose, and to my wife, Asma, whose continuous support kept the work moving along. This thesis could not have been finished without these people.

Finally, I wish to acknowledge the financial support of the National Superconducting Laboratory throughout my graduate studies.

**TABLE OF CONTENTS**

## LIST OF FIGURES

## LIST OF TABLES

# CHAPTER 1

## INTRODUCTION

### 1.1 Superconducting Cavities

Superconductivity has become an important technology for particle accelerators. Radio frequency superconducting cavities (SRF) have been operating routinely for many years in a variety of accelerators for high-energy physics, low-energy to medium-energy nuclear physics research, and free-electron lasers. A key component of the modern particle accelerator is the device that imparts energy to the charged particles. This is the electromagnetic cavity resonating at a microwave frequency at very low temperatures where the material of the cavity is electrically super-conducting. For more information on super-conductivity refer to appendix 5.4 to this report.

### 1.2 Thermal Breakdown

Thermal breakdown, commonly known as "Quench", is a phenomenon that occurs in the accelerating cavity due to a rise in the temperature of the cavity, in a small localized region known as a "defect". With the increase in rf power, these sub-millimeter-sized regions that have rf losses substantially higher than the surface resistance of an ideal superconductor, grows and become normal conducting regions. Hence, the result is sudden loss of power in the accelerating field $E_{acc}$. The two most critical design features of a super-conducting accelerating cavity are its average accelerating field, $E_{acc}$, and the quality factor $Q_o$, which is the intrinsic Q of the resonant cavity defined as the. ratio of the energy stored (U) in the cavity to the energy lost ($P_c$) in one rf period. This thermal breakdown (quench) is a mechanism that ultimately limits field strengths, $E_{acc}$, in superconducting cavities whose microwave performance is not affected by multipactoring (a resonant process in which a large number of electrons build up within a small region of the cavity surface) or field emission (emission of electrons from high electric field regions of the cavity). [1]. It is now a well-known fact that this effect takes place within a localized, point-like region of the cavity inner surface rather than over a large fraction of the super-conducting areas. At these localized regions, therefore, the temperature continues to rise with the increase in RF power input and could eventually cross the critical temperature ($T_c$), which may result in a quench condition [1].

1.3 Past Research

Thermal breakdown in superconducting RF cavities is one of the limiting factors in achieving high values of average accelerating field ($E_{acc}$). Thermal breakdown originates at sub-millimeter-size regions that have RF losses substantially higher than the surface resistance of an ideal superconductor.

K.R. Krafft et al. have studied the mechanism of thermal-magnetic breakdown in super-conducting cavities by systematically investigating the two most important thermal transport phenomena in the cavity-cooling bath system: the thermal conductivity of the metal and heat transport across the metal to liquid helium interface. They concluded that the thermal transport in super-conducting niobium cavities is determined by the interplay of the temperature dependant functions of the surface resistance, thermal conductivity, and the metal to liquid helium thermal boundary resistance [2].

H. Padamsee et al. have investigated the behavior of thermal breakdown through the construction of a phenomenological model by considering it as a purely thermal effect. They found that the factors influencing the production of heat at the defect are the defect size and resistance. Also, the surface resistance of the metal determines the additional power dissipated in the neighboring super-conducting niobium. They developed 1-D computer simulations to model thermal-magnetic breakdown by incorporating heat production as well as heat transportation factors. Essentially, the program calculates the temperature of the defect and vicinity for increasing RF field levels until the thermal breakdown takes place [1].

R. Romijn, W.Weingarten and H.Piel have presented calibration measurement for the temperature mapping system in use at European Organization for Nuclear Research (CERN) for super-conducting acceleration cavities immersed in sub-cooled liquid helium. They concluded, from their experiment, that the resistor thermometer response on a heat source at the cavity interior surface could be described by turbulent convection heat flow [4].

H.P. Kramer et al have discussed the heat transfer from technical copper to flowing He II for different heat fluxes and different flow velocities. They argued that since the theory of Kapitza conductance can at best account for the heat transfer from specially treated ultra-clean surfaces, heat transfer from "dirty" technical surfaces still has to be described empirically. He found that the heat transfer coefficient of liquid helium II does not depend on the flow velocity [3].

# CHAPTER 2

## NUMERICAL SIMULATIONS

### 2.1 Model Definition

The SRF cavity is modeled as a rectangular parallelepiped 3-D surface, as shown in Figure 1

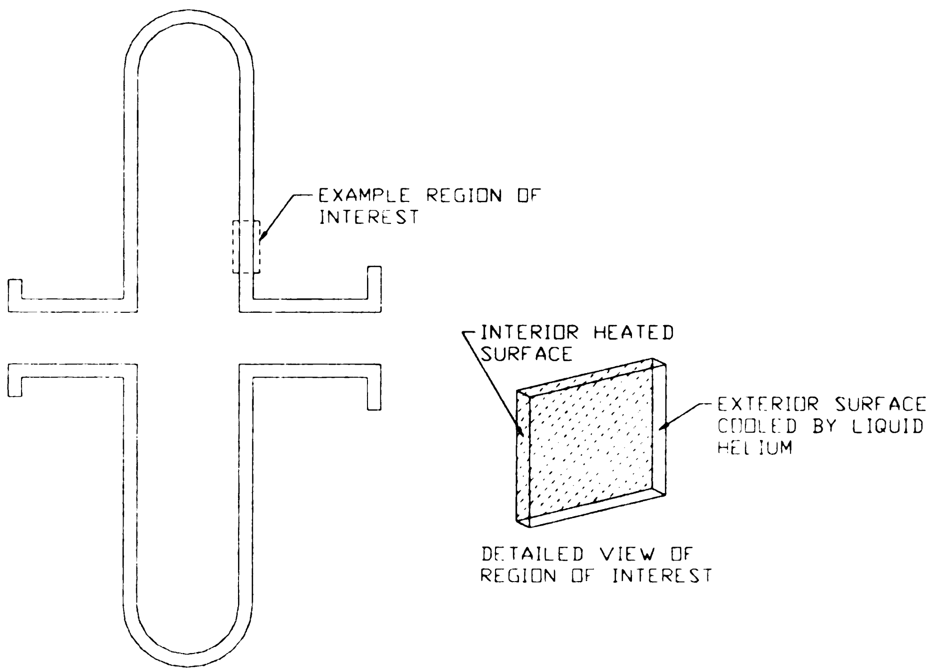


Figure 1 Region of interest on an elliptical super-conducting cavity is modeled as a rectangular parallelepiped surface with point of heat source on the interior surface and cooled by the liquid helium on the exterior surface

This section of the cavity is chosen to be representative of the whole cavity. A more elaborate view of this three dimensional surface with sensors installed on one face, known as cold surface, is shown in Figure 2

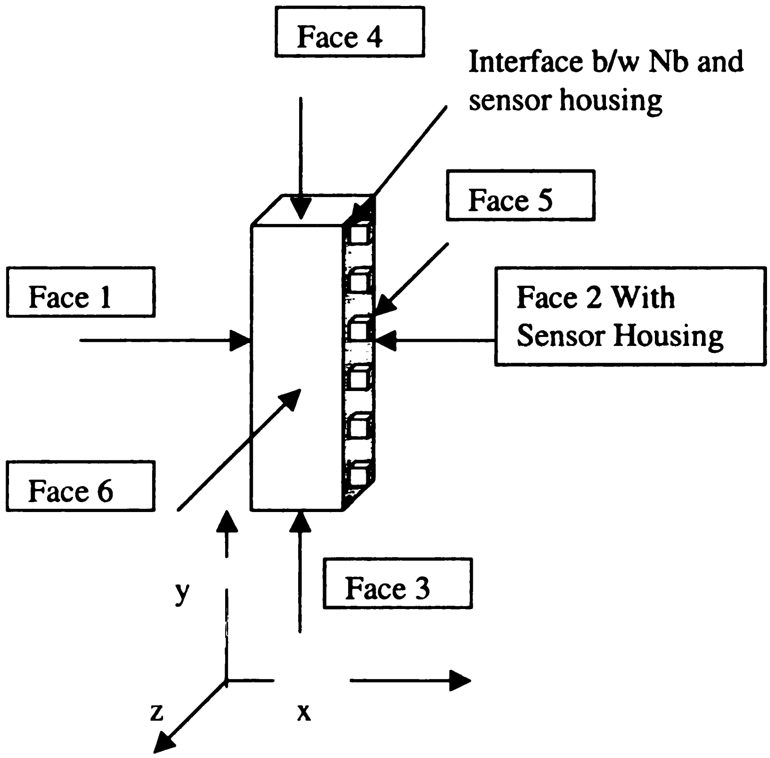


Figure 2 Rectangular parallelepiped surface has point of heat source on face 1 and sensors installed on face 2 where liquid helium is to cool down the whole cavity to the desired operating temperature. x-axis is chosen in the direction of thickness of the niobium metal.

## 2.2 Assumptions in Model

In order to describe the heat transfer behavior in the niobium cavities, mathematical modeling is done to relate it with the actual physical phenomena. This mathematical model is based upon certain underlying assumptions, which are discussed below:

### Steady State Heat Conduction

Since thermal breakdown in SRF cavities is a phenomenon that limits the $E_{acc}$ of the cavity, accurately computing the steady state temperature distribution is of prime importance. Also from a typical order of magnitude analysis, the transient time constant, known as Fourier number ($F_o = \frac{\alpha t}{L_c^2}$), is quite large, even for small times of several milliseconds, and steady state conditions are reached very rapidly. In this relation, $\alpha$ is the thermal diffusivity of the niobium in ($\frac{cm^2}{\sec}$), $L_c$, is the characteristic length i.e. thickness of the niobium in (cm) and, t is time in (sec). Moreover, since the present study is focused upon finding the optimum sensor spacing as a function of detectable temperature rise above ambient, a steady state solution to the problem is more desirable.

Since there is no heat being generated inside the niobium, the equation for transport of heat across the niobium surface can be simplified. Point heating has been assumed on the inner surface of the cavity. Since no finite heating source can be described as point heating, a single grid point of heating is assumed to model the point heating behavior.

Since the operating temperature of the cavities is below the critical temperature of the niobium ($T \leq T_c$) where $T_c \cong 9.2\ ^o k$ for niobium the Meissner effect [12] dictates that the magnetic field does not affect heat conduction in the niobium. Transport of heat out of the cavity through radiation is considered to be negligible as compared with convective heat transfer through liquid helium.

Though the insulated sensor housings are made with several materials, the main composition of the sensor that has any significant role in transportation of heat is the casing of the sensor. This is made of G-10 material, a kind of epoxy filled fiberglass.

Due to the low thermal conductivity of the G-10 sensor housing, the contact resistance with the niobium is neglected. Moreover, this contact resistance is further reduced by applying a thin film of varnish (IM-7031) that has low electrical conductivity but high thermal conductivity at low temperatures. The use of this varnish, thus allows us to neglect the interface resistance without significant loss of accuracy.

## 2.3 Governing Differential Equation

Based upon the assumptions described above, the heat transport equation in the SRF cavity material is described as:

$$\frac{\partial^2 T}{\partial X^2} + \frac{\partial^2 T}{\partial Y^2} + \frac{\partial^2 T}{\partial Z^2} = 0 \qquad 2.1$$

This differential equation in three dimensions, is commonly known as the 'Laplace Equation' and is categorized as elliptical in nature.

The boundary conditions on each of the six faces are described with respect to the faces identified in Figure 2. Since there are two distinct material surfaces in the problem, i.e. niobium plate and the material of the sensor, the boundary conditions are described accordingly.

2.3.1 <u>Boundary Conditions on the Niobium Surface</u>

(a) <u>Face 1; at x=0. (Heated Face)</u>

There are two boundary conditions (a mixed boundary condition) specified on Face 1.

$$q\big|_{y.z(Pt.heat)} = \text{User specified}$$

$$q\big|_{y.z(excipt\ Pt.heat)} = 0$$

Heat flux is zero on all grid points except on one single grid point (input by the user) where flux q is specified in $Watts/mm^2$.

(b) <u>Face 2; at x= L ( cooled surface)</u>

This face also has two types of boundary conditions i.e. mixed boundary conditions: -

(i) Surface with no sensor

$$q\big|_{No\,sensor} = h_{conv,He}\,\Delta T$$

(ii) Surface with sensors

$$q\big|_{Nb} = q\big|_{Sensor}$$

$$T_{Nb(i,j,k)} = T_{Sensor(i,j,k)}$$

Here L is the thickness of the niobium plate.

(c) Faces 3 & 4; at y=0,W

$$\frac{\partial T}{\partial y} = 0$$

Here, W is the width of the niobium plate

(d) Faces 5 & 6; at z=0,H

$$\frac{\partial T}{\partial z} = 0$$

Here, 'H' is the height of the niobium plate

2.3.2 Boundary Conditions on the Sensor

Since the whole sensor is assumed to be immersed in the liquid helium, a convective boundary condition, as given below, is valid for the five sides of the sensor.

$$q\big|_{sensor} = h\big|_{conv,He}\,\Delta T$$

The boundary condition on the sixth surface of the sensor i.e. at the interface with the niobium surface is same as described for the niobium surface and is repeated here for completeness.

$$q_{Nb}\big|_{x=L} = q_{Sensor}\big|_{x=L}$$
$$T_{Nb(i,j,k)} = T_{Sensor(i,j,k)}$$

Here 'L' is the thickness of the niobium plate.

## 2.4 Discretization of the Differential Equation

The discretization of the differential equation is done using a finite difference technique. The second order differentials in the equation are discretized at a point by using the central difference with respect to the two neighboring grid points. Hence the scheme is second order accurate.

$$\frac{T_{i-1,j,k} - 2T_{i,j,k} + T_{i+1,j,k}}{\Delta x^2} + \frac{T_{i,j-1,k} - 2T_{i,j,k} + T_{i,j+1,k}}{\Delta y^2} + \frac{T_{i,j,k-1} - 2T_{i,j,k} + T_{i,j,k+1}}{\Delta z^2} = 0 \qquad 2.2$$

This discretized equation, which is now a simple algebraic equation, can be solved through SOR (Successive Over Relaxation) iterative technique.

Solving for $T_{i,j,k}$, we get

$$T_{i,j,k} = \frac{1}{\lambda}[\alpha(T_{i-1,j,k} + T_{i+1,j,k}) + \beta(T_{i,j-1,k} + T_{i,j+1,k}) + \gamma(T_{i,j,k-1} + T_{i,j,k+1})] \qquad 2.3$$

Where,

$$\lambda = 2(\Delta x^2 \Delta y^2 + \Delta x^2 \Delta z^2 + \Delta z^2 \Delta y^2)$$

$$\alpha = \Delta y^2 \Delta z^2$$

$$\beta = \Delta z^2 \Delta x^2$$

$$\gamma = \Delta y^2 \Delta x^2$$

This equation is a Gauss-Seidel method representation of the Laplace equation. Introducing the convergence acceleration parameter $\omega$, this equation converts to an SOR representation of the three-dimensional Laplace equation.

$$T^{n+1}_{i,j,k} = T^{n}_{i,j,k} + \omega[\frac{1}{\lambda}\{\alpha(T^{n+1}_{i-1,j,k} + T^{n}_{i+1,j,k}) + \beta(T^{n+1}_{i,j-1,k} + T^{n}_{i,j+1,k}) + \gamma(T^{n+1}_{i,j,k-1} + T^{n}_{i,j,k+1})\} - T^{n}_{i,j,k}] \qquad 2.4$$

Here the superscripts"n+1" is the current iteration number and "n" is the previously computed iteration number.

"$\omega$" varies between 1 and 2 and is determined through numerical experimentation to enhance the convergence. For $\omega=1$, the equation reduces to equation (2.3), the Gauss-Seidel iterative method.

2.5 Implementation of Boundary Conditions

At the boundaries, since one of the two end surface grid points is not defined in the central differencing scheme, a hypothetical point is assumed to exist beyond the surface boundary. The relation for the hypothetical point is then derived from discretization of the known boundary condition, which is then substituted into the equation (2.4) for that point. It is also realized that except at the interface boundary of niobium plate with the sensor, all boundary equations developed through this technique are similar to the ones that can be obtained by applying finite control volume approach. In the following sub paragraph, this principle is applied to implement the corresponding boundary conditions and one boundary equation is derived from both these methods to illustrate this similarity.

2.5.1 On Heated Face

At Face 1 on the point of heating, the boundary condition is specified as:

$$q = -k_{Nb} \frac{\partial T}{\partial x} ,$$

Here the grid point $T^{n+1}_{i-1,j,k}$ is the hypothetical point, as 'i-1' doesn't exist on the surface. To find the relation for this point, the above boundary condition can be expressed algebraically with central difference as

$$q = -\frac{k_{Nb}}{2\Delta x}(T_{i+1}^{n+1} - T_{i-1}^{n})$$

or $$T_{i-1,j,k}^{n+1} = \frac{2q\Delta x}{k_{Nb}} + T_{i+1,j,k}^{n}$$

Hence the complete boundary equation becomes

$$T_{i,j,k}^{n+1} = T_{i,j,k}^{n} + \omega[\frac{1}{\lambda}\{\alpha(\frac{2q\Delta x}{K_{Nb}} + 2T_{i+1,j,k}^{n}) + \beta(T_{i,j-1,k}^{n+1} + T_{i,j+1,k}^{n}) + \gamma(T_{i,j,k-1}^{n+1} + T_{i,j,k+1}^{n})\} - T_{i,j,k}^{n}] \quad 2.5$$

Now applying the finite control volume approach to the same boundary point, we get:-

$$K_{Nb}(\frac{\Delta x\Delta z}{2\Delta y})(T_{i,j+1,k} - T_{i,j,k}) + K_{Nb}(\frac{\Delta x\Delta z}{2\Delta y})(T_{i,j-1,k} - T_{i,j,k})$$
$$K_{Nb}(\frac{\Delta x\Delta y}{2\Delta z})(T_{i,j,k+1} - T_{i,j,k}) + K_{Nb}(\frac{\Delta x\Delta y}{2\Delta z})(T_{i,j,k-1} - T_{i,j,k})$$
$$K_{Nb}(\frac{\Delta y\Delta z}{\Delta x})(T_{i+1,j,k} - T_{i,j,k}) + q\Delta y\Delta z = 0$$

After simplification to solve for $T_{i,j,k}$, we get

$$T_{i,j,k} = \frac{1}{\lambda}\{\alpha(\frac{2q\Delta x}{K_{Nb}} + 2T_{i+1,j,k}^{n}) + \beta(T_{i,j-1,k}^{n+1} + T_{i,j+1,k}^{n}) + \gamma(T_{i,j,k-1}^{n+1} + T_{i,j,k+1}^{n})\}$$

Here $\alpha$, $\beta$ and $\gamma$ are the same as used in equation (2.4).

Hence it is seen that this equation is exactly the same as equation 2.5 once assembled in SOR technique. This shows that the two methods of applying the boundary conditions results in similar boundary equations.

Similarly, for the boundary points where heat flux is zero, the relation for a hypothetical point is developed as:

$$q = 0 = -k_{Nb} \frac{\partial T}{\partial X}$$

which results into $T^{n+1}_{i-1,j,k} = T^{n}_{i+1,j,k}$

2.5.2 Convective Boundary Condition

The convective boundary condition is given by working on the similar principle:

$$q = -k_{Nb} \frac{\partial T}{\partial x} = h_{He}(T_{Nb} - T_{\infty}),$$

Here $T_{Nb}$ is the temperature at the niobium-helium interface and $T_{\infty}$ is the known bulk temperature of the liquid helium. When central differenced, the relation becomes:

$$T^{n}_{i+1} = T^{n+1}_{i-1} - \frac{2\Delta x h_{He}}{k_{Nb}}(T^{n}_{i} - T_{\infty})$$

2.5.3 Boundary Condition at the Niobium-Sensor Interface

On the interface boundary between the niobium surface and the G-10 material of the sensor housing, as shown in figure 2, the boundary condition can be expressed more easily with the help of a finite control volume approach and is expressed as:

$$\begin{aligned}
&\frac{\Delta y \Delta z}{\Delta x}(k_{Nb} + k_{G-10})T_{i,j,k} - \frac{\Delta y \Delta z}{\Delta x}(k_{Nb}T_{i-1,j,k} + k_{G-10}T_{i+1,j,k}) + \\
&\frac{\Delta x \Delta z}{\Delta y}(k_{Nb} + k_{G-10})T_{i,j,k} - \frac{\Delta x \Delta z}{\Delta y}(k_{Nb} + k_{G-10})(T_{i,j-1,k} + T_{i,j+1,k}) + \\
&\frac{\Delta y \Delta x}{\Delta z}(k_{Nb} + k_{G-10})T_{i,j,k} - \frac{\Delta y \Delta x}{\Delta z}(k_{Nb} + k_{G-10})(T_{i,j,k-1} + T_{i,j,k+1}) = 0
\end{aligned}$$

Solving for $T_{i,j,k}$ and simplifying the equation we get,

$$T_{i,j,k}^{n+1} = \frac{1}{\lambda}[\alpha\{(\frac{2k_{Nb}}{k_{Nb}+k_{G-10}})T_{i-1,j,k}^{n+1} + (\frac{2k_{G-10}}{k_{Nb}+k_{G-10}}) T_{i+1,j,k}^{n}\} + \beta(T_{i,j-1,k}^{n+1} + T_{i,j+1,k}^{n}) + \gamma(T_{i,j,k-1}^{n+1} + T_{i,j,k+1}^{n})] \qquad 2.5$$

Here $\alpha$, $\beta$ and $\gamma$ are the same as used in equation (2.4).

If a close look at this equation is made, it becomes evident that this equation is quite similar to equation (2.4) except for the coefficients of the x-direction terms, which now have the influence of the thermal conductivities of the two materials. This can also be seen if we simplify this equation with the thermal conductivities of the two materials is made equal, the equation becomes the same as equation 2.4 for one homogeneous material. Hence a convenient and simple logic is found to implement this boundary condition along with the other boundary conditions into the computer program.

2.5.4 Other Sides of Boundary Conditions On Sensor Housing

Since we are dealing with a three dimensional case, the sensor housing must have five other surfaces in addition to the one mentioned in the case of Face 2. If the sensor is not on any of the side edges then all other five faces shall have same type of convective boundary condition as described above in 2.5.2 and is given as:

$$q = h_{He}(T - T_{\infty})$$

But if any sensor is modeled on the edge or corner of the niobium surface, then this side of the sensor shall have the insulated boundary condition. So, if the sensor is aligned with the top or bottom surface, then the valid boundary condition imposed as:

(a) $\frac{\partial T}{\partial y} = 0$ and,

If the sensor is aligned with the edges of face 5 or face 6, then

(b) $\frac{\partial T}{\partial z} = 0$

2.5.5 Boundary Conditions on Face 3 and 4

These faces are modeled as insulated surfaces, and the boundary condition is given as:

$\frac{\partial T}{\partial y} = 0$, then

$T^{n+1}_{i,j-1,k} = T^{n}_{i,j+1,k}$ for face 3 and,

$T^{n+1}_{i,j+1,k} = T^{n+1}_{i,j-1,k}$ for face 4.

2.5.6 Boundary Conditions on Face 5 and 6

These faces are also modeled as insulated surfaces, since no heat transfer takes place across them. So the boundary condition is given as: -

$\frac{\partial T}{\partial z} = 0$, then

$T^{n+1}_{i,j,k-1} = T^{n}_{i,j,k+1}$ for face 5 and

$T^{n+1}_{i,j,k+1} = T^{n+1}_{i,j,k-1}$ for face 6

2.6 Program Characteristics

2.6.1 Convergence

Numerical formulation of Laplace equation can be represented in a system of linear algebraic equations. These algebraic equations can be written in the matrix form with $\bar{U}$ representing the solution vector.

A $\bar{U}=\bar{E}$

The solution of this system of equations exists and is unique if and only if A is non-singular, in which case

$\bar{U}=A^{-1}\,\bar{E}$.

It may be shown that the following conditions are sufficient for the Gauss-Seidel methods of iteration to converge [13]:

(a) The n x n matrix A is irreducible.

(b) $a_{ii} > 0$

(c) $\sum_{\substack{j=1 \\ j \neq i}}^{n} \left| a_{ij} \right| \leq a_{ii}$, with strict inequality holding for at least one value of 'i'.

It is observed that the system of algebraic equations arising from the application of equation 2.4 along with the boundary conditions described above in section 2.5 satisfy the above conditions of convergence.

Defining the value of epsilon sets the convergence criterion for the program. The program scans the whole grid to find the absolute largest 'difference value' on the entire grid between the previous value and the newly computed value at the corresponding grid point. It then compares this largest 'difference value' with the user defined epsilon value. If this largest difference value over the whole computational domain is greater than the epsilon, the program continues for the next iteration otherwise, it displays the indication of convergence. The value of epsilon is selected by the user depending upon the number of significant digits to which the accuracy is desired in the solution. Smaller values of epsilon would require a greater number of iterations to converge and hence require more computing time. Also, it is important to note that, if the solution already contains very small numbers, then the value of epsilon must be selected such that it is significantly lower (depending upon accuracy desired to the number of significant digits) than the smallest value expected in the solution domain. This can be done through obtaining an initial-guess solution by test running the program on a coarse grid with smaller domain size. From this guess-solution, the smallest value in the solution is used to Figure out the value of epsilon that shall provide the desired accuracy in the actual solution. The default value of epsilon used in the program is $10^{-6}$.

### 2.6.2 Post Processing

As shown in Figure 3, the highest temperature locations on the cooled surface are the four corners where sensors are installed because of the relatively reduced cooling effects of the liquid helium. Due to the relatively high thermal conductivity of niobium at low temperatures, heat generated by a point source is conducted away diffusively within the metal and a very low temperature rise is expected at the outer surface of cavity. Moreover, the rise in temperature on the cooled surface to be detected by the sensors is greatly influenced by the excellent cooling properties of superfluid helium. Figure 8 shows the relation between the sensor efficiency and the sensor spacing for different thickness sizes of the niobium plate. Sensor efficiency is a function of distance between the sensors (sensor spacing) and can be defined as the ratio of temperature sensed by the sensor on the cooled surface and the maximum temperature on the inner surface of the niobium cavity. The program is repeated for each thickness of niobium plate i.e. 1mm and 4 mm and for each value of selected bulk temperature of liquid helium i.e. 2 K and 4 K, for varying sensor spacing in each case.

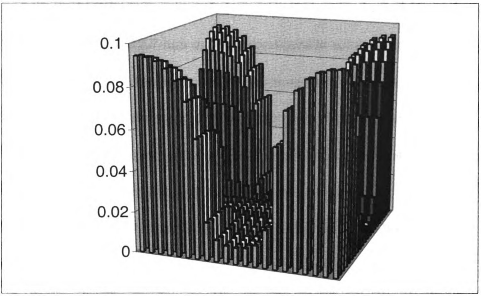


<u>Figure 3</u> Program output showing most heated spots at the four corners under the sensor locations

2.6.3 <u>Program Verification</u>

Code verification is done with the results obtained through the exact solutions generated by COND3D, developed for Sandia National Laboratory [15] and through the Kokopelli Finite Element Method program developed for Los Alamos National Laboratory [16]. As shown in Figure 8, the results obtained from all three programs are in good agreement with each other and the error is within 1% of the exact solution.

2.6.4 <u>Program Validation</u>

The validity of the model is assured by comparing the results obtained from the program with the experimental data. Since no past experiment with similar boundary conditions is known to exist, an independent experiment was performed at room temperature. Six thermocouples as shown in Figure 4, were used to record the temperature of the cold surface of a 4mm thick niobium plate. A thin foil heater of 12.7 mm diameter was used to act as the point heating source for the problem. The bottom surface, the hot surface, was then insulated using two G-10 sheets of different thicknesses. The thin sheet (approx 0.5-1.0mm) was flexible enough to bear against the bottom surface of the niobium plate with the heater sandwiched between the two. Then, the thick (approx 20-30 mm) sheet of G-10 was placed under the thin sheet to further insulate the bottom of the niobium surface. An insulation 'duct' tape was used to bond the three plates together which also provided insulation to the side walls of the niobium plate to match the boundary condition as close to the model as possible. The experimental data thus obtained is then compared with the data obtained from the program. As shown in Figure 4a, the two results are in agreement with each other. The standard deviation in difference of the two results is 0.009427°C

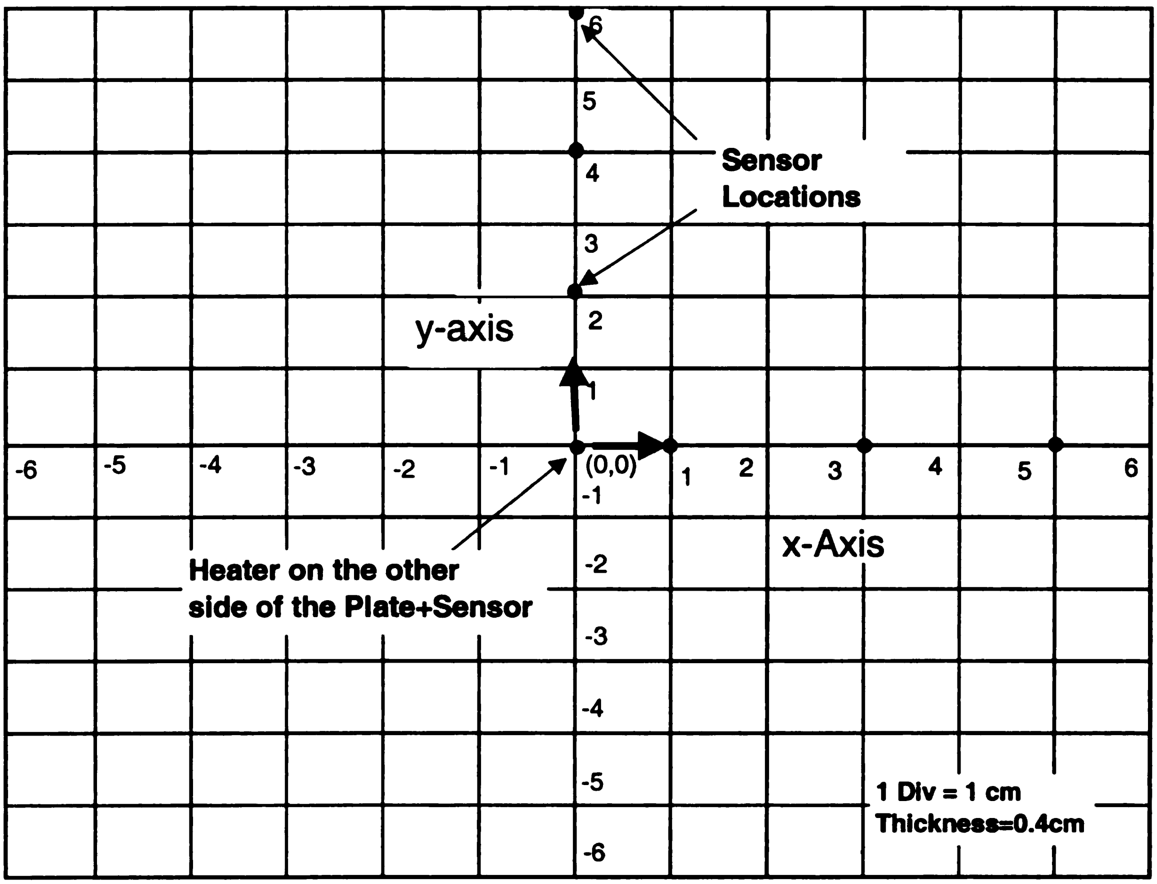


Figure 4 Experimental setup to validate the computational model. Six sensors placed 1 cm apart over a 4 mm thick niobium plate with heater installed on the bottom surface.

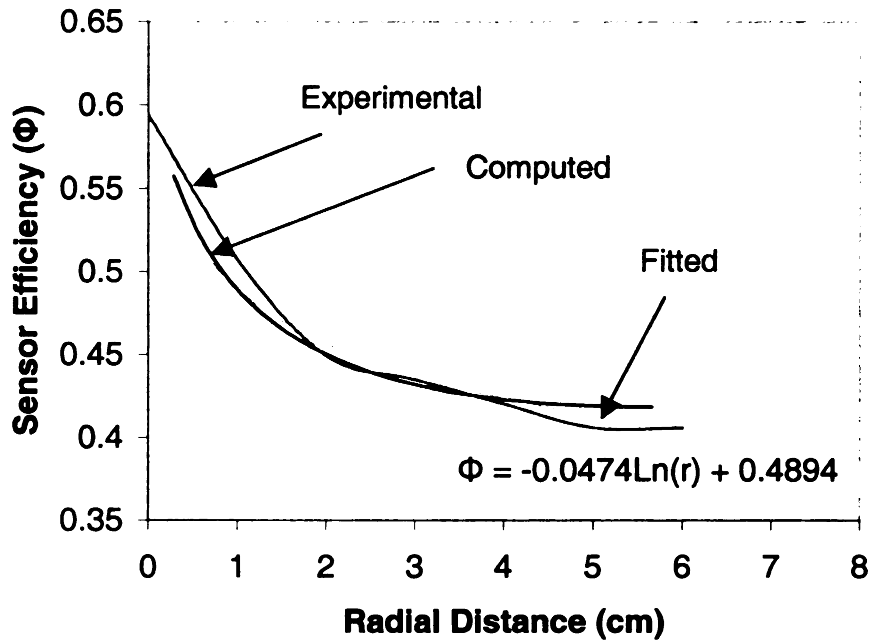


Figure 4a Sensor efficiency (Φ) shown as a function of radial distance (r). The relationship obtained from numerical computation is compared with the one obtained from the experimental setup at room temperature

2.6.5 Verification through Inverse Heat Conduction Calculations

To verify the results obtained from the program, yet another weapon in the arsenal is the inverse heat conduction calculations through parameter estimation. Here the parameters are the unknown temperature at the niobium surface right under the heater and the '*x*' and '*y*' coordinates of the heater. Since in this experiment we know the actual parameters before their estimation, the accuracy of the results obtained from this technique may provide a good level of confidence; especially, once it is applied during the actual operation of the cavity where these parameters would not be known a priori. The equation employed in this method, and the result thus obtained, are described briefly below.

From the definition of sensor efficiency i.e. the ratio of temperature at the sensor to the maximum temperature on the heated surface , we know that

$$\Phi(r) = T(r) / T_{max}$$

where, $\Phi(r)$ is the sensor efficiency and is function of distance 'r' which itself is given as

$$r = \sqrt{(x - x_i)^2 + (y - y_i)^2}$$

here, $(x,y)$ is the unknown location of the heat source and $(x_i,y_i)$ is the known location of the sensor 'i' over the plate

$T_i$, is the temperature at a distance 'r' measured by the sensor '$i$', and

$T_{max}$ is the unknown maximum temperature on the heated surface of the plate i.e. at the point of source of heating.

In matrix form this equation can be written as

$$[T_i] = T_{\max}[\Phi(r_i)]$$

In this equation, as described above, $T_{max}$, and the coordinates $(x_i,y_i)$ of the heater (which determines the value of $r_i$ ) are the unknowns. Now if we have, let us say six temperature sensors installed on the top (cold) surface of the plate to detect the heat produced by the heater on the bottom (hot) surface of the plate, then each sensor shall have its efficiency curve as a function of its location 'r' away from the point of heating. Such a curve for each sensor is obtained from the direct computation through the 3-D steady state program output. Thus from the above equation, we shall have following six set of equations,

$T_1 = T_{max}\,\Phi(r_1)$

$T_2 = T_{max}\,\Phi(r_2)$

.

.

$T_6 = T_{max}\,\Phi(r_6)$

Now, in this set of six equations, we have just three unknowns. So we have an over-defined set of equations whose unique solution doesn't exist. However, through parameter estimation software written by Dr Robert L. McMasters, unknown variables with optimum best (least square sense) values can be obtained through a non-linear least squares technique. These values ($x_i$, $y_i$ and $T_{max}$) can then be obtained using the functional form of $\Phi(r_i)$ through the direct solution.

Thus the close agreement of the two results as shown in Table 1 validates the potential of estimation of parameters through inverse heat conduction methods. The values of estimated parameters are then used to calculate the temperature rise detected by each sensor. The difference between the measured temperature rise from the sensor and the calculated temperature rise is quite small with standard deviation of only 0.045 Kelvin.

| Verification of Estimated Parameters through Inverse Technique | | | | |
|---|---|---|---|---|
| **x** | **y** | **Measured Temp Rise** | **Estimated Temp Rise** | **Error** |
| 1 | 0 | 3.5 | 3.43799008 | -0.062 |
| 0 | 2 | 3.1 | 3.104853539 | 0.0048 |
| 3 | 0 | 3 | 3.039895125 | 0.0399 |
| 0 | 4 | 2.9 | 2.899929045 | -7.095E-05 |
| 5 | 0 | 2.8 | 2.863678044 | 0.0637 |
| 0 | 6 | 2.8 | 2.774763514 | -0.0252 |
| | | | **Std.Dev (K)** | 0.0449 |
| | **Parameter** | | | |
| | **Estimated** | **Experimental** | | |
| **Max Temp Rise (K)** | 6.89735 | 6.9 | | |
| **x (cm)** | 0.222 | 0 | | |
| **y (cm)** | -0.278 | 0 | | |

Table 1 Showing difference between actual temperature rise and estimated temperature rise at sensor location by using estimated parameters.

## 2.7 Results and Discussion

The result shown in Figure 9 shows the variation of sensor efficiency with the sensor spacing. At low sensor spacing for a particular sensor, high sensor efficiency can be achieved. However, it has been previously stated [9] that a signal of 60 μK can be resolved with a higher scanning time. So, from this result, we can assume a signal of 60 μK from which we can find a corresponding sensor spacing. For example, sensors on the cooled surface of a 1 mm thick niobium plate and at bath temperature of 2 K can be placed at a spacing 4 cm distance apart and will be able to detect a 1K-temperature rise anywhere in the material. Similarly, at 4 k the sensors on a 4 mm thick niobium plate can be placed at a distance of almost 13 cm apart. The essential requirements to apply this technique during the actual operation of the cavity have also been carried out and are described in the subsequent chapters.

# CHAPTER 3

# THERMAL PROPERTIES OBTAINED FROM THE LITERATURE

## 3.1 Literature Search

A significant amount of effort has been expended to extract thermal property data for niobium metal and liquid helium at extremely low temperatures. Since very little information is available about materials at such low temperatures in standard data books, much of the information is obtained through research papers published in various journals and other publications.

### 3.1.1 Thermal Conductivity of Niobium

As shown in Figure 5 [3], the thermal conductivity of niobium metal depends on the RRR value of niobium metal, which is a measure of metal purity. As the graph shows, there is a sharp decrease in the curve below $T_c$=9.2 K. However, the higher the RRR value, the higher the thermal conductivity. As discussed in chapter 3 of reference [9], the reason for these features is that electrons are the dominant carriers of heat. Though, the phonons (lattice vibrations) also play a role in heat conduction, but this is significant only at T<4 K. Below $T_c$, the thermal conductivity drops sharply as more electrons condense into Cooper pairs. Because the depairing energy is not available from random thermal motion, the pairs are not scattered by the lattice vibrations and therefore cannot conduct heat from one part of the niobium to another. At high temperatures (4 k < T < $T_c$ ), a significant, though small, fraction of electrons is not frozen into Cooper pairs and can carry heat effectively, provided that the electron-impurity scattering is low. As electrons condense into Cooper pairs, electron-phonon scattering also decreases. Below about 4 K, the thermal conductivity from phonons dominates and begins to increase, leading to the phonon peak near 2 K. With decreasing temperature, the number of phonons decreases $\propto T^3$. Ultimately the value of the phonon conductivity maximum is limited by phonon scattering from lattice imperfections, of which grain boundary density is the most important. If the crystal grains of niobium are very large, because of annealing at high temperature, one observes a large phonon peak, as shown in the thermal conductivity behavior of the sample with RRR=250, which was annealed at 1400 °C [9].

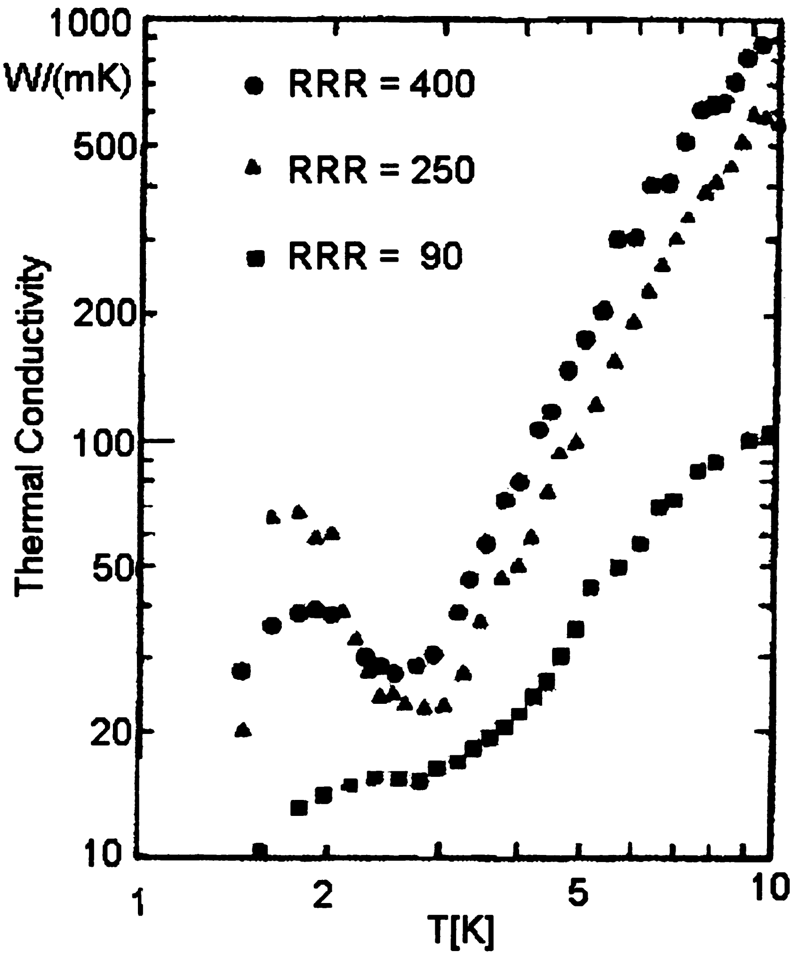


Figure 5 Thermal conductivity of niobium at low temperatures

### 3.1.2 Thermal Conductivities of Common Cryogenic Materials

The thermal conductivity values of some commonly used materials are given in Figure 6 for a wide range of temperatures from around 1 °C to 300 °C on a logarithmic scale [5]. Thermal conductivity of G-10, an epoxy filled fiberglass material, is also shown in this Figure which is a poor conductor of heat at low temperatures.

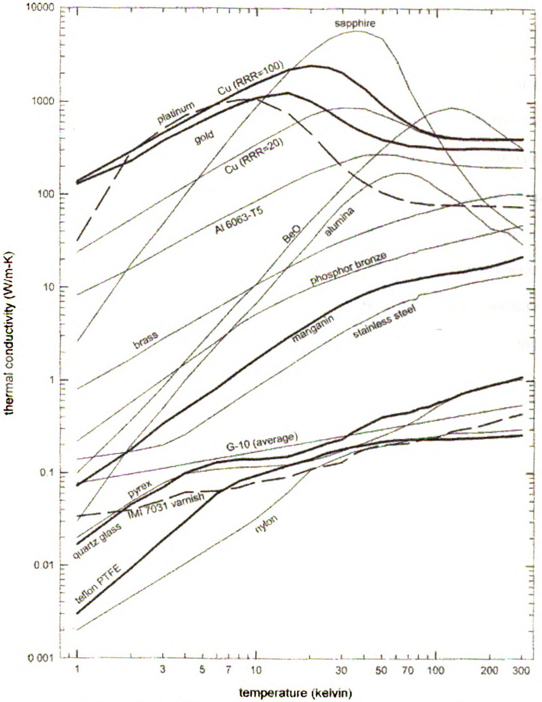


Figure 6 Thermal conductivity of G-10 and other materials commonly used in cryogenic environment

### 3.1.3 Convection Heat Transfer Coefficient For Liquid Helium

Unlike thermal conductivity, the heat transport across a solid-liquid helium interface is not well understood [9]. Kramer et al. have found the experimental value of the convection heat transfer coefficient of liquid helium for a temperature range of 1.5 °K to 2.3 °K as shown in Figure 7 and 8 [3]. Figure 7 shows the variation of heat transfer coefficient with temperature. An important conclusion drawn from this Figure is that the heat transfer coefficient of helium II is the same for system pressures 0.1 and 0.25 Mpa. Also, while crossing the lambda transition temperature of helium i.e. the temperature at which phase change take place between normal liquid helium and the superfluid helium (See appendix 5.2 for more details), the heat transfer coefficient drops to about 30 % of its previous value.

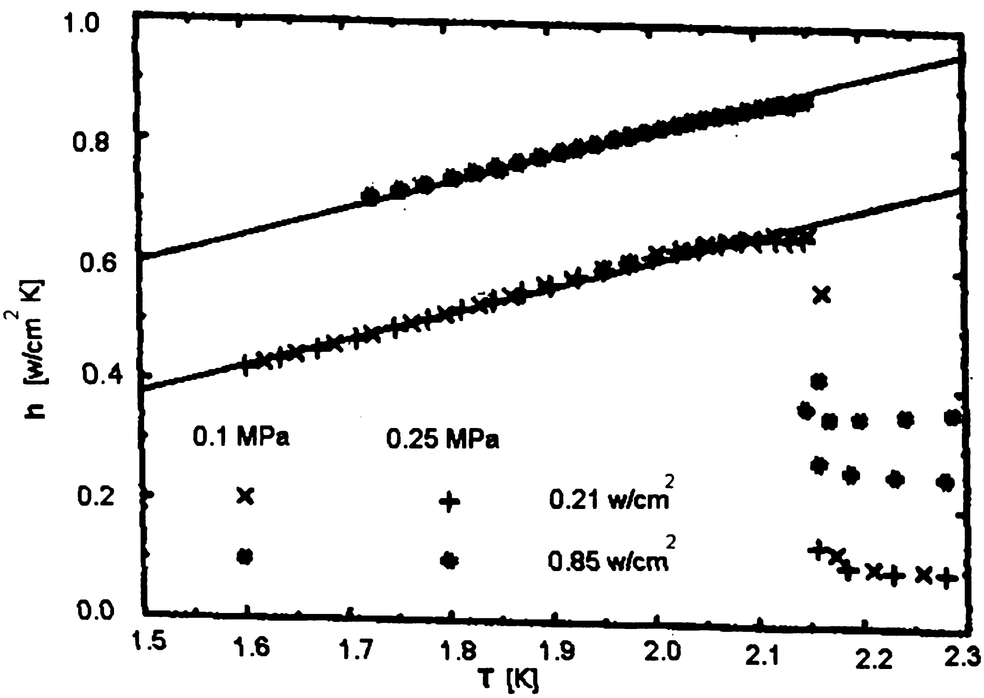


Figure 7 Variation of heat transfer coefficient with temperature for two values of heat flux at two different pressures

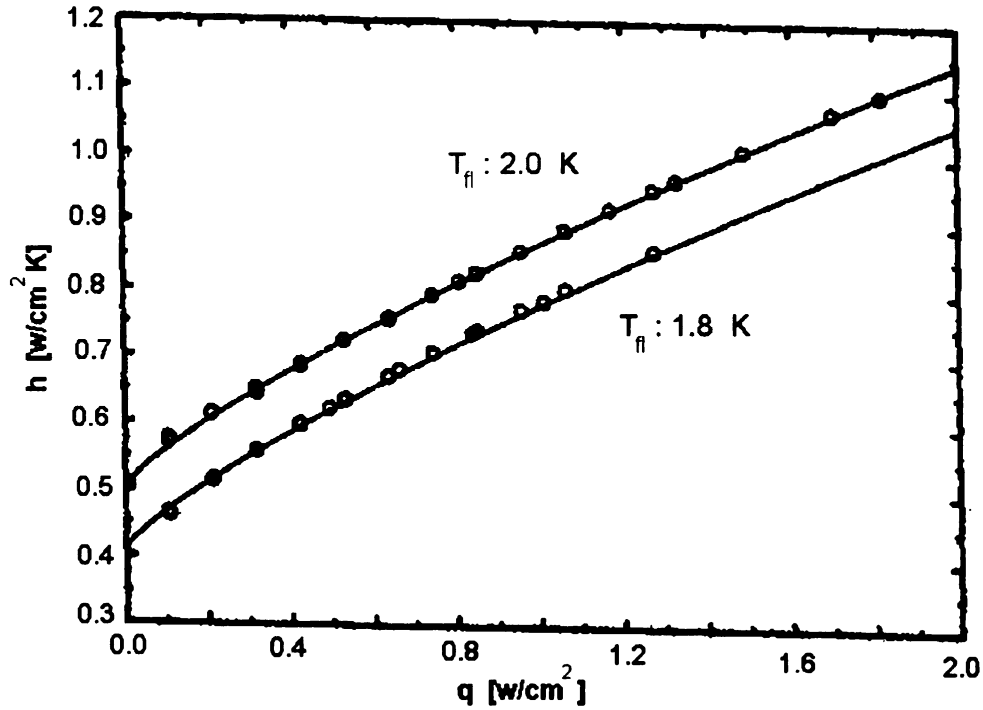


Figure 8 Variation of heat transfer coefficient with heat flux for the specific case of two bulk helium temperatures, i.e. for 1.8 K and 2.0 K

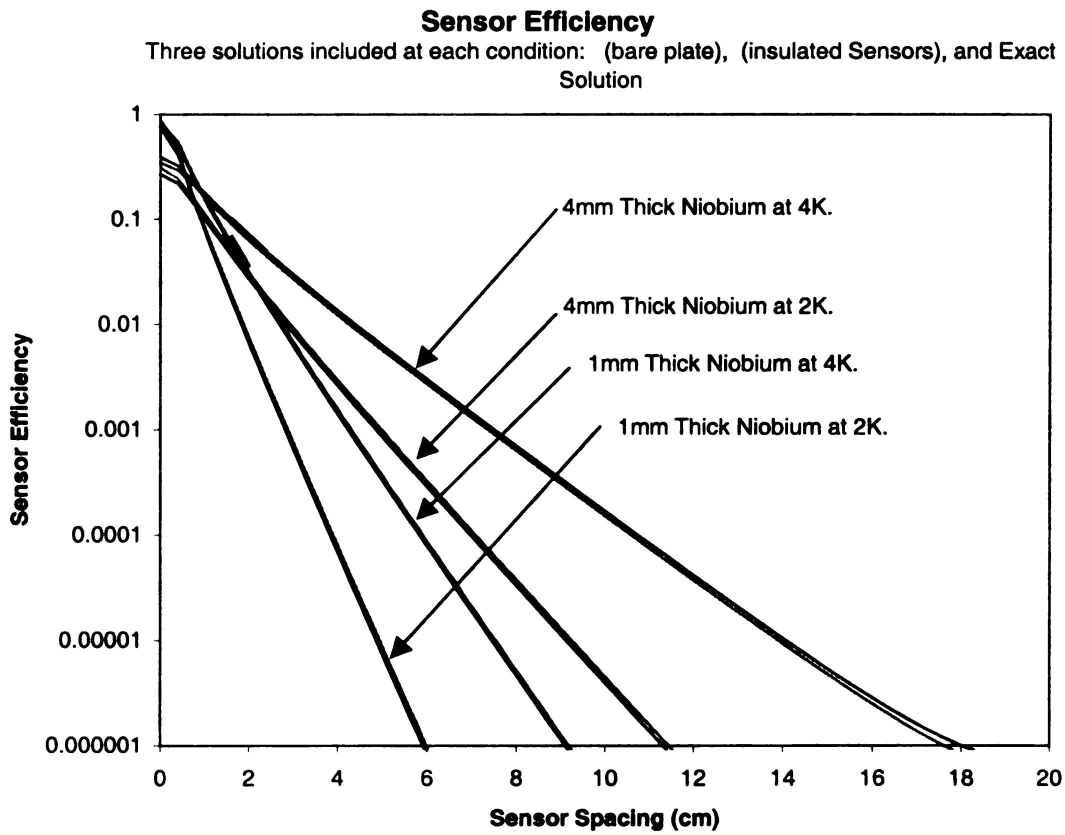


Figure 9 Sensor efficiency as a function of sensor spacing

# CHAPTER 4

## EXPERIMENTAL STUDIES

### 4.1 Thermal Sensor Design and Manufacture

Since the operation of the SRF cavity is around 2 Kelvin, at which the liquid helium is a super-fluid (liquid helium at temperatures below its phase transition i.e. 2.17 K, doesn't change to solid but remains a liquid known as super fluid. For more information refer to appendix 5.2 to this report), it is important to have special design features, which may enable the sensors to monitor the temperature rise above the bulk temperature of the liquid helium. Previous studies at Cornell University [9] have demonstrated that a signal of 60 μK above ambient can be resolved through a careful design of carbon resistor temperature sensors. However, in the Cornell study, it is maintained that, because of the excellent cooling characteristics of the superfluid helium in which the thermometers are immersed, the efficiency of the sensors is greatly reduced from 100 % of the wall temperature to about 20-30%. Here, again sensor efficiency is defined as the ratio of the detected temperature increase to the actual rise in wall temperature. Consequently, they used a large number of fixed thermometers to cover the whole cavity. Typically, for a 1.5 GHz single cell cavity almost 700 thermometers would be required [9]. The focus of the present study, however, is to estimate the appropriate sensor spacing required to detect a temperature rise of 1 °K above ambient anywhere on the inner surface of niobium cavity.

The basic design features of the sensors used in this research are essentially the same as those developed at Cornell University [6] and manufactured in the same way. However, the sensor installation procedure on the single cell cavity is somewhat modified as described in the subsequent paragraphs.

4.1.1 Sensor Selection

A sensor selection criterion is based upon the following considerations: -

- High sensitivity especially at low temperatures.
- Insulated from liquid helium.
- Insensitive to magnetic or ionization fields.
- Simple in design and low cost.

Though the selection of 1/8 watt, 100 ohm Allen Bradley carbon resistor and its housing (capsule) design is based upon the one already used at Cornell University [6], the present study tries to quantify the sensor selection properties through thermal analysis.

4.1.2 Sensor Manufacture

The sensor manufacturing procedure used in this research is also based on the guidelines used at Cornell University and involves, typically, the following processes: -

- Manufacturing of sensor housing with G-10 material as shown in Figure 10.
- Spot welding of resistor leads with 36 AWG 'Manganin wire'.
- Epoxy filling of the housing with resistor held in middle of the housing.
- Observing the epoxy curing time.
- Grinding the epoxy from the top of the housing to expose the heat sensitive carbon element of the resistor.

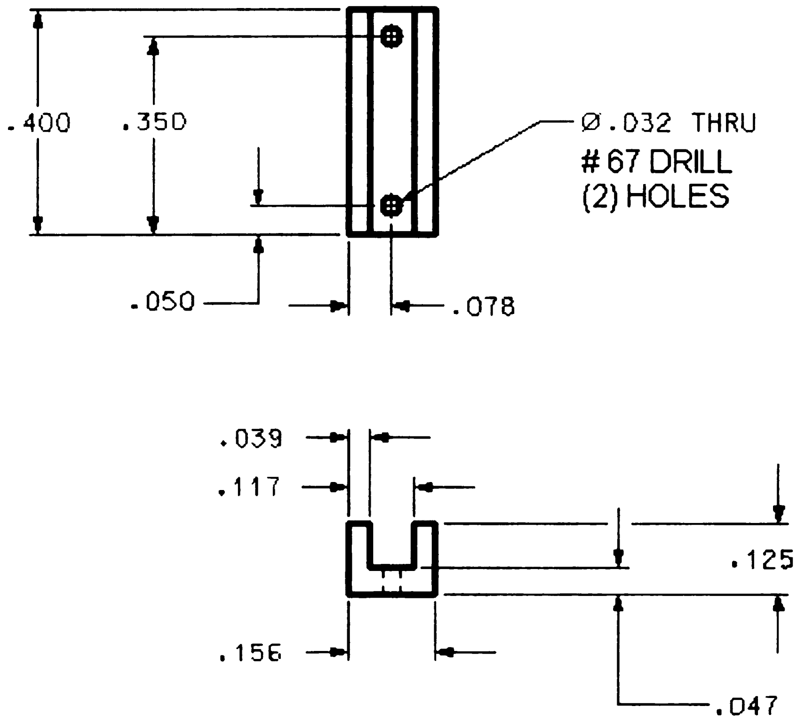


Figure 10 Drawing details of sensor housing

4.2 Sensor Design Issues

The sensor selection and its manufacturing has been done on the basis of past experiences of Cornell University, however, the order of magnitude analysis to estimate the relative heat transfer from such a sensor into the surrounding liquid helium is provided in the subsequent paragraphs.

4.2.1 Cooling Effects on Sensor

Cooling of the carbon element inside the sensor housing can be attributed to the two main sources i.e. cooling through the sides of the housing and cooling through the manganin wires. The estimates for the cooling of the sensor are based on a 1 K rise in temperature above the ambient temperature, which is a much larger temperature rise than any actually encountered, providing a conservative estimate of heat loss.

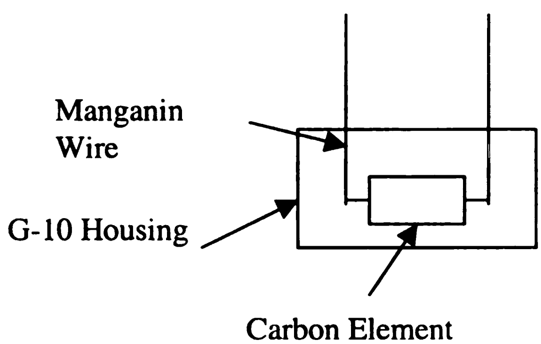

### 4.2.2 Cooling of Sensor Through G-10 Housing

From Fourier's Law of heat conduction, we know that

$$Q = -kA\frac{\Delta T}{\Delta x},$$

Where, Q is the heat transfer from the sensor to the liquid helium

$\Delta$T is 1 K (i.e. one degree rise in temperature) above ambient.

'K' is the thermal conductivity of the G-10 material at 4 K

'$\Delta$x' is the wall thickness of the G-10 material

'A' is the surface area of the sidewall of G-10 exposed to liquid helium.

So, the heat transfer from one surface, Q = $5.29\times10^{-4}$ Watts

Hence, the total heat transfer from all the 5 surfaces of the sensor that are exposed to the liquid helium is, Q = $2.43\times10^{-3}$ Watts.

### 4.2.3 Cooling Effect On The Sensor Through Manganin Wire

For simplicity and applying a more conservative approach, this problem is divided into two parts:

(a) Assuming the whole portion of wire outside the G-10 housing is at the same temperature as that of liquid helium. Hence, the effective temperature difference (i.e. 1 degree difference in temperature) takes place on the length of wire between the sensor and the edge of G-10 housing.

For AWG-36 wire having diameter of 0.36 mm,

$Q = 2.227\times10^{-5}$ Watts (2 Wires)

$Q = 4.454\times10^{-5}$ Watts (4 Wires)

(b) Heat transfer from the length of the wire inside the liquid helium, can be taken as a typical case of heat transfer through fins. The solution is available in standard textbooks on heat transfer. Interestingly, the total heat transfer through the wire of infinite length is

$Q = 5.162E^{-4}$ Watts for 2 Wires, and

$Q = 1.032E^{-3}$ Watts for 4 Wires.

4.2.4 <u>How much is infinite length?</u>

For the conditions stated in part (b), the infinite length i.e. the length of fin at end of which the heat transfer is effectively zero and temperature of the fin is the same as the temperature of the fluid, is computed from the following fin equation [13]:

$$Q = \sqrt{hPKA_c}\,(T_o - T_\infty)\tanh\left(\sqrt{\frac{hP}{KA_c}}\,L\right)$$

For infinite length $\tanh\left(\sqrt{\frac{hP}{KA_c}}L\right) = 1$

Or $\tanh\left(\sqrt{\frac{hP}{KA_c}}L\right) \cong .99$

$$L \geq \sqrt{\frac{KA_c}{hP}}\,(2.65)$$

Where $k$ is the thermal conductivity of the wire.

'A' is the cross sectional area of the wire.

'h' is the convective heat transfer coefficient of liquid helium.

'P' is the circumferential perimeter of the wire.

Substituting in the values for these parameters, we get, L ≥ 0.363 mm

This effective length of wire, in which any significant heat transfer is taking place, is a small number. This is because, beside the extremely small cross sectional area of the manganin wire, liquid helium has a very high convective heat transfer coefficient as compared to the low thermal conductivity of the manganin wire at 4 K. Hence, nearly all the heat coming out of the wire from the edge of the G-10 housing, is convected away within this length of wire. The rest of the length of wire has nearly no effect on cooling the sensor.

In view of the two comparisons, we can observe that the cooling of the sensor through the manganin wires is not significant as compared with the cooling of the sensor from the G-10 sidewalls.

4.2.5 Ohmic Self Heating of the Sensor

For resistance temperature detector (RTD) type sensors, ohmic self-heating is a known problem which occurs especially when using negative RTDs (resistor whose resistance increases as temperature goes down). The monitoring instrument used in the experiment is from LakeShore® Inc. model 218 and can display a maximum resistance of 7.2 KΩ. Since the instrument provides a constant current of 10 μamps, the maximum resistance of the sensor the instrument can display limits maximum power dissipated inside the resistor. This power dissipation can be computed from the following relation:

$$P = I^2 R$$

Where 'P' is the dissipated power

'I' is the current of the instrument, and

'R' is the resistance of the sensor.

Once the power is known, rise in sensor temperature due to this dissipated power can be calculated from the relation:

$\Delta T = Q/(h\,A)$,

Where, Q is the dissipated power,

'h' is the convective heat transfer coefficient of liquid helium, and

'A' is the surface area of the sensor.

From this relation, the estimates for rise in temperature of sensor due to self-heating are given in table 2.

| Helium Temp (K) | Current Source ($\mu$ Amps) | Power ($\mu$ Watts) | $\Delta T$ ($\mu K$) |
|---|---|---|---|
| 4.0 | 10 | .18 | .59 |
| 2 | 10 | .75 | .98 |

Table 2 Thermal analysis of ohmic self-heating. Here, delta t is the rise in sensor temperature due to self heating.

## 4.3 Sensor Installation / Mounting System

### 4.3.1 The Tree

The installation procedure used in this experiment is fundamentally different than the one used at Cornell. Instead of using pogo sticks on the sensors and using G-10 board to map these sensors onto the contour of the cavity from the top iris to the equator and to the bottom iris, a simple but more versatile design is used. This design, as shown in Figure 11, has been specifically selected so that it can be applied to a wide variety of shapes of cavities as well as on multi-cell cavities without any major modification in the basic design. The sensors on this design pattern, called a Tree pattern, are equally spaced in both radial and transverse directions. The 'Tree' can be mounted on any one of twelve cavity support bars. Since these support bars are equally spaced at 30 degrees, a maximum of 12 such trees can be mounted for one side (either the top or bottom) surface of the cavity. Each tree, then has two radial rows of sensors, called the branches, with each having 4 to 5 sensors depending upon the desired spacing between the sensors. As shown in Figure 12, manganin wires from each sensor on the branch of a tree can be attached to their respective 'D-type' connectors installed for each branch on the tree.

### 4.3.2 Ribbon Cables

Normal ribbon cables take the temperature signal of the sensor from the D-connectors to the 'Feed Through' on top of the cryogenic Dewar as shown in Figure 14.

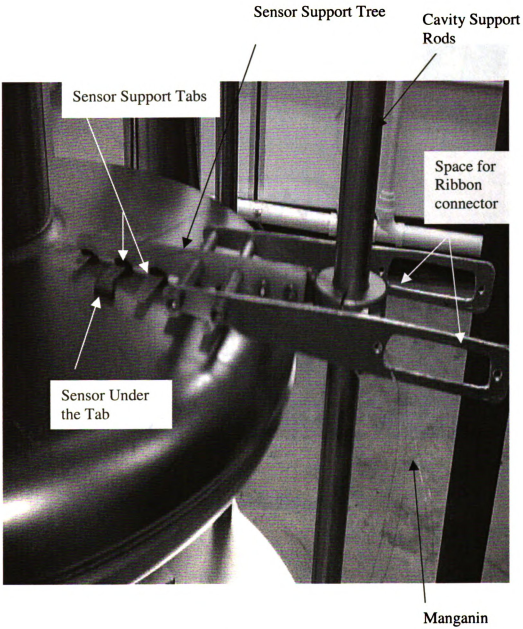


Figure 11 Sensor installation tree

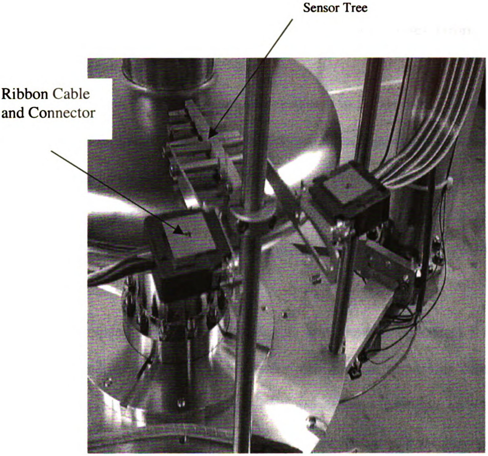


Figure 12 Sensor installation tree (2)

## 4.4 Sensor Measurements Technique

### 4.4.1 Four-Lead Measurement

The four-lead measurement technique eliminates the effect of lead resistance on the measurement. If it is not accounted for, lead resistance causes errors in the temperature measurements.

As shown in Figure 13, a two lead sensor is shown in a four lead measurement technique. In this configuration, the current leads and voltage leads run separately to the sensor. With separate leads, there is little current in the voltage leads so their resistance does not enter into the measurement, whereas resistance in the current leads will not change the current as supplied by the constant current source.

### 4.4.2 Measurement of Two-Lead Sensors

Due to limited space in a congested cryogenic environment, sometimes it is not possible to have the luxury of having four wire measurement sensors as described above. However, it is possible to use a four wire measurement technique on a sensor with two leads coming out of the cryogenic dewar. Four-lead sensor measurement in this situation, can be adopted by attaching the plus voltage to plus current and minus voltage to minus current leads at the back of the vacuum feed through on top of the cryogenic dewar. The error in such a resistive measurement is the resistance of the lead wire run with current and voltage together inside the cryogenic dewar. This resistance may have to be traded off using the two lead measurements for a greater number of sensors inside the dewar.

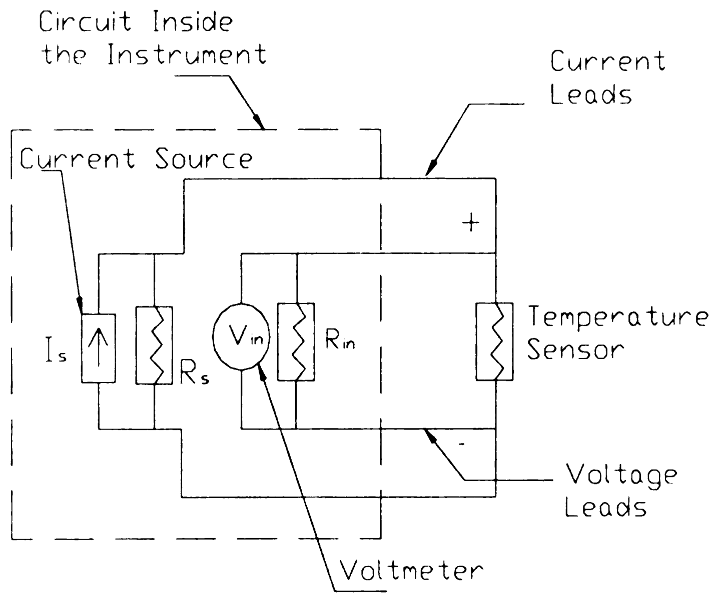


<u>Figure 13</u> **Four lead sensor measurement technique**

### 4.5 Design And Manufacture Of Vacuum Feed-Through.

Since the number of wires going into the cryogenic Dewar is always limited by the capacity of the feed-through as well as the capacity of the pipe and passages from where the bundle of wires has to pass, a good design for a Vacuum Feed –Through is always important. Many off-the-shelf vacuum feed-throughs are available from different vendors, but none was considered sufficient to meet the specified requirements. For example, a commonly used six-way multiple connector conflat® type vacuum feed-through is not only expensive but also has a limited capacity of only 100 wires. Moreover, it requires special connectors on the vacuum side wire connections, which themselves may incur extra cost. It was for this reason an ingeniously designed feed-through is used (Manufactured by Mr. Steve Bricker of NSCL) as shown in Figure 14.

This feed-through has a capacity of 240 wires in a conflat type vacuum seal. It has a total of 10 connectors of 24-pin standard 'CPC AMP' type for the airside connections and a D-type connector with ribbon cables on the vacuum side connections.

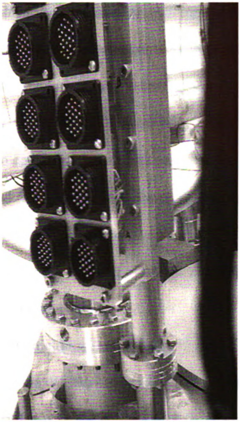

Figure 14 Vacuum feed-through having ten amp-cpc connectors, twenty-four pins each

## 4.6 Design Criteria For Data Signal Cables.

The data signal cables used outside the cooling system can be much different from those used inside. Between the instrument and the feed-through, heat leak is not a problem. Error and noise pickup is minimized by the use of the following criteria for the selection of data signal cables. The cable shall be

- Twisted pair (to cancel out inductance noise)
- Braided or foil shielded (to reduce noise pickup from external sources or environment)
- Larger conductor i.e. 22 to 28 AWG stranded copper wire. (flexible but maintaining low resistance)

### 4.6.1 Grounding And Shielding Sensor Leads

Since the sensor input measurements are not isolated from ground, sensor lead cables are not grounded with the outside chassis of the instrument [5]. Shielding the data signal cables is important to keep external noise from entering the measurement. A shield is most effective when it is near the measurement potential. The instrument used in this experiment is Model 218 from LakeShore® Inc. and offers a shield that stays close to the measurement potential. Therefore, the shield pin in the connector of the data signal cable is connected to the input connector shield pin of the model 218 instrument. However, the other end of this shield pin in the data signal cable is not connected to ground or to the instrument chassis or in the cooling system.

## 4.7 Signal Processing

Signal processing is done within the instrument model 218. The instrument has two groups of eight input channels. Each group must have the same input type. The instrument has 8 (one for each input channel) constant current sources to provide an excitation current of 10 $\mu$ Amperes for each sensor. It employs four-lead differential measurement for each input channel and the measurement of this experiment from the RTD sensor is displayed in ohms. The range the instrument can display is 0 to 7500 ohms.

The instrument has two A/D converters to provide 16 new readings per second. Therefore the display rate is twice each second. Though the measurement resolution of the unit is 50 m$\Omega$ but the display resolution is limited to 100 m$\Omega$.

### 4.8 Data Logging

Data logging is done on a standard IBM compatible PC with the help of a serial interface connection with the instrument model 218. A program has been under use at NSCL (developed by Alberto Rodriguez) to log data from each sensor onto the hard disk of the computer. A file can be generated either in Microsoft Excel or HTML file format to save the data. The program has a user selectable data logging rate which can log the data as fast as approximately 237 ms, which is faster than the data acquisition rate of the temperature monitor.

### 4.9 Sensor Calibration.

The accuracy of a sensor relates to how closely the measurement of resistance can be converted to temperature relative to some recognized temperature scale. Understanding how the accuracy of temperature sensors is specified begins with the definition of the response curve, i.e. Resistance vs. Temperature for the carbon resistor sensor. Though some sensors follow a known standard response within a given tolerance, carbon resistor sensors must be calibrated to determine their response curve. Therefore, the carbon resistor sensors are not interchangeable or at least require calibration after installation.

We know that the accuracy of a sensor is determined by the stability of the sensor and the system in which it is calibrated. Calibration of carbon resistor sensors, in this experiment, is done with respect to a standard Germanium resistor sensor that is pre-calibrated from factory standard settings (ITS-90) and can be traced back to NIST.

In the calibration procedure, data is collected for the variation in resistance of the carbon sensors with respect to the change in temperature recorded by the Ge sensor as shown in Figure 15. Since the fitted curve is very close to the experimental curve, therefore no significant variation in the two curves can be seen in Figure 15. However, Figure 16 shows the residuals present in the polynomial fit to the calibration curve. The fourth order polynomial

$$T = A + BR^{-1} + CR^{-2} + DR^{-3} + ER^{-4}$$

ıs then fitted to the experimental data.

The parameters A, B, C, D, and E are computed to fit the experimental data and hence yield a standard deviation of 0.003789 Kelvin.

Now, once the relation is known, other pertinent relation for data analysis can be obtained very easily. For example the sensitivity of the carbon sensor can be obtained by differentiating the above equation as: -

$$\frac{dT}{dR} = -BR^{-2} - 2CR^{-3} - 3DR^{-4} - 4ER^{-5}$$

The relation used at Cornel University is given as:

$$T = \frac{1}{A\ln(R) + \frac{B}{\ln(R)} + C}$$

This relation requires only 3 unknown parameters to be found, but is not trivial to solve since it is a non-linear relation, especially once sensitivity calculations require the differential of this relation.

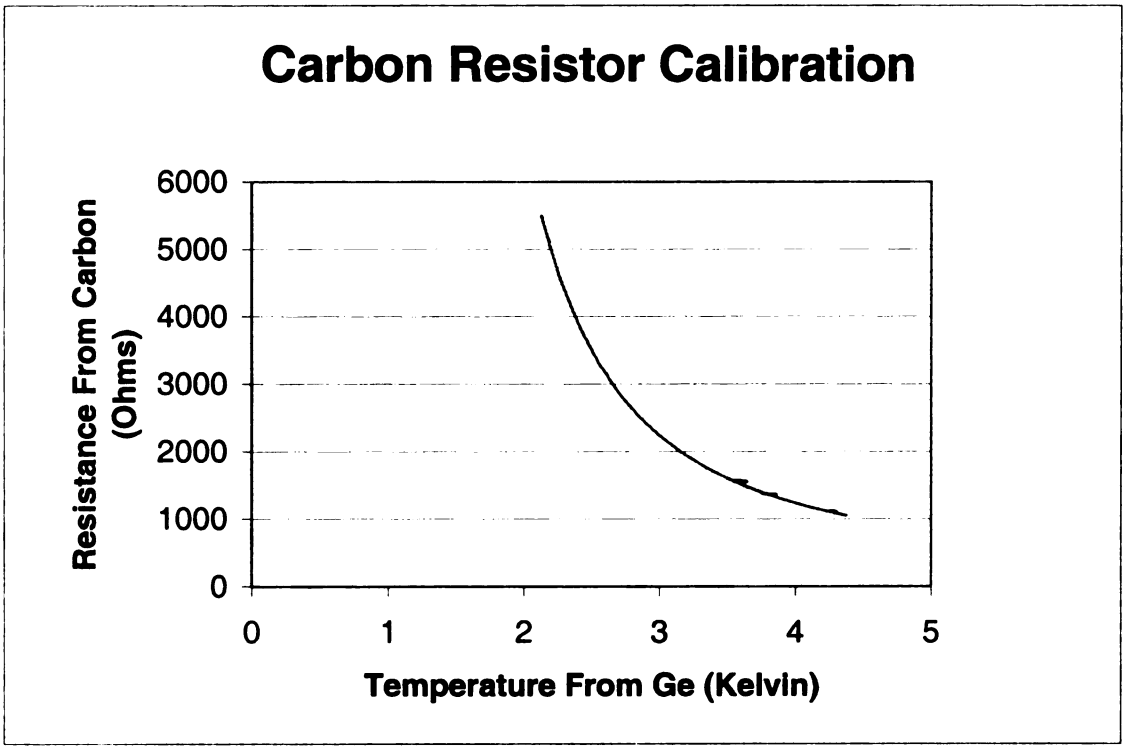


Figure 15 Calibration curve for carbon sensor resistance as a function of temperature based on a germanium sensor

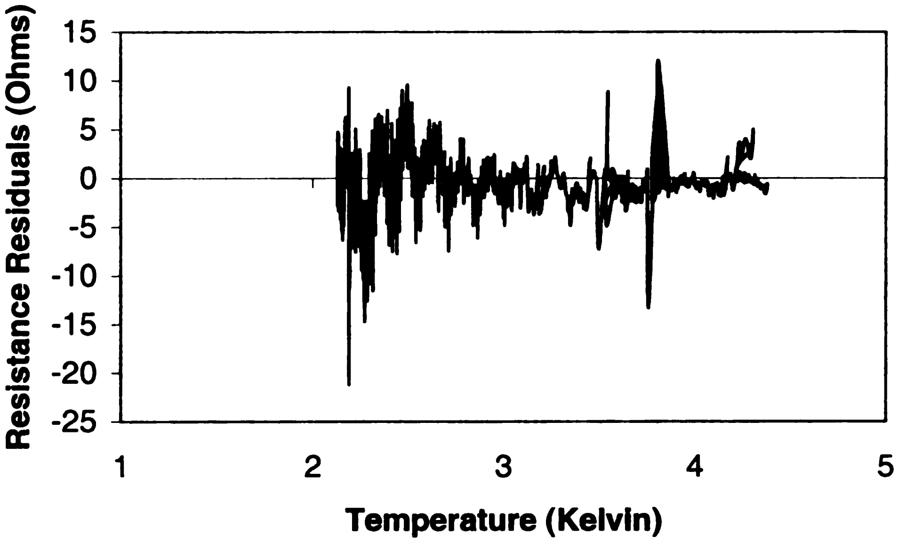


Figure 16 Residual of polynomial fit to the calibration data

4.10 Sensor Sensitivity and Measurement Resolution.

A typical calculation is performed on sample data, as shown in Table 3, which is obtained from the calibration curve of a carbon resistor. The comparison of sensitivity between the Germanium and the Carbon resistor shows that, at low temperatures, the Carbon resistor is more sensitive than the Ge resistor especially once the temperature goes down from 4 °K to 2 °K. The chart also indicates that the Carbon sensor at 2 K, with the given monitor display resolution, is sensitive enough to resolve a heat signal of 9.4 μK.

| **Sensor Type** | | **Germanium** | **Carbon** |
|---|---|---|---|
| **Temperature Coefficient** | | Negative | Negative |
| **Monitor Display Resolution** | | 100 mΩ | 100 mΩ |
| **Sensor Sensitivity at** | 4 K | -116.98Ω/K | -572 Ω/K |
| | 2 K | -930.04 Ω/k | -10537.8 Ω/k |
| **Monitor Display Resolution w.r.t. 100 mΩ** | 4 K | 854 μK | 174 μK |
| | 2 K | 107.52 μK | 9.4 μK |

Table 3 Sensor sensitivity and display resolution of the sensor monitor

# APPENDICES

## 5.1 Program Description

### 5.1.1 User Graphical Interface (UGI)

To simulate the thermal model of the super conducting cavity into a computer program, 'Visual Basic' as a programming language is used. The advantage of this language over other high level languages is that Visual Basic, besides being as fast as others, has a system by which a graphical interface can be generated much more easily. This added advantage of a better graphical interface results in providing a professional appearance to the program and provides a more 'user friendly' environment. The first window, where the user interacts with the program, commonly known as user graphical interface or simply the UGI, has some text boxes along with some option buttons for the input by the user. Two command buttons allow the user to either execute the program with a 'Start' button, or abort the program with a 'Cancel' button.

### 5.1.2 Input Text Boxes of UGI

Input text boxes of UGI are the places where the user can describe the dimensions of the model. These dimensions include the configuration of the niobium plate i.e. thickness (x overall dimension), height (y overall dimension) and, length (z overall dimension) and the configuration of the sensors installed on the cold surface of the niobium plate i.e. thickness of the sensor (height), length and width of the sensor. Moreover, flexibility in the design for the placement of sensors is also incorporated. This is done by allowing the user to define the distance, as per design requirement, between the base of the niobium plate and the bottom surface of the first sensor. This distance is zero in case the two surfaces i.e. base of the niobium plate and the bottom surface of the sensor, are in-line with each other.

Depending upon the number of grid points required by the user in the numerical problem, values of delta x, delta y and, delta z can also be prescribed in this UGI.

The UGI not only facilitates the user to define material properties required by the program such as thermal conductivities and heat transfer coefficient of the materials involved, but also allows for prescribing the location and the amount of point heating flux on to the heated surface of niobium plate, so that physically correct boundary conditions can be implemented in the program

Flexibility of choosing the desired accuracy for the convergence of the solution is also built into the program by allowing the user to prescribe the value of epsilon in one of the input text boxes. The default value is $10^{-10}$.

During the program execution, iteration numbers are displayed with an increment of 20 iterations, to indicate the processing of the program.

### 5.1.3 Option Boxes of the UGI

Option for applying SOR to the scheme is left at the discretion of the user by providing an option button. This button is checked for SOR by default and if unchecked the scheme will become an ordinary Gauss-Seidel iterative procedure. If the SOR option is utilized, value of omega=1.8 is used to accelerate the convergence of the program. It is estimated that, in using this option, the program can reduce the number of iterations to almost one fifth of the time required by the ordinary Gauss-Seidel iterative method with no loss of accuracy.

Since the sensors are rectangular in shape, their orientation with respect to the niobium plate coordinates can also be prescribed. The user can optionally choose the orientation of the sensors by placing the width of the sensor to be either aligned with the y-direction or with the z-direction.

A word of note is also displayed on the GUI, at the bottom right corner of the screen; to remind the user for selecting consistent units while designing the input values for the problem. The results would be meaningless if units for different dimensions are not kept consistent.

### 5.1.4 Program Listing

The computer program code developed in Visual Basic® is given below to implement the mathematical model described in chapter 2.

```
Option Explicit
' 3-D STEADY STATE HEAT CONDUCTION PROBLEM IN A PARRALLELPIPED
'DOMAIN WITH POINT HEATING ON HEATED SURFACE AND SENSORS
'INSTALLED ON THE SURFACE COOLED BY LIQUID HELIUM.

Dim Lx As Single  'Overall dimension in the x direction
Dim Ly As Single 'Overall dimension in the y direction
Dim Lz As Single  'Overall dimension in the z direction
Dim omega As Double

Dim Dx As Single 'Delta x
Dim Dy As Single 'Delta y
Dim Dz As Single 'Delta z

Dim strMyDataString As String
Dim strInputDataString As String
Dim blnsensel As Boolean
Dim seldec As Integer
Dim txt11 As String
Dim txt12 As String
Dim tloop As Integer
Dim consttl As Double        ' Defined as = dt/(rho*cp*dx) for left b.c (constant flux)
Dim constt2 As Double        ' Defined as = 2*alpha*dx*h/k for right b.c (convective)

Dim KNb, Kg10, Hf, Tf 'constants of thermal conductivity, convective heat coefficient
'of fluid, Fluid temperature T(infinity),(Rho, Spht not requried)

Dim Alpha, Beta, Gama, Nue 'Computed Constant Coefficients in all three dimensions
Dim Index As Integer
Dim q As Double
Dim YinQ, ZinQ, sor As Integer
Dim imx As Integer  'Mx limit if no sensor found in x-dir
Dim imax As Integer 'Mx limit if sensor found in x-dir
Dim jmax As Integer
Dim kmax As Integer

Dim postop() As Single
Dim poslft() As Single

' Dimensions of sensors
Dim Hs, Ls, Ws As Double
Dim Ytotsen, Ztotsen As Integer

Dim Zbase, Ybase, ytop, ztop As Double

Dim Zgap, ygap As Double
```

```
Dim qygp, qzgp As Integer

Dim YSize, ZSize, intfac As Double
Dim Nygps, Nygpg, Nygpb, Nzgps, Nzgpg, Nzgpb, YsenNUM, ZsenNUM As Integer
Dim zsentbl() As Integer
Dim ysentbl() As Integer
Dim Ysensr, Zsensr, flag As Boolean
Dim ZsLL, ZsUL, YsLL, YsUl As Integer


Dim itr As Integer
Dim Errmx As Double
Dim Error As Double
Dim Epsilon As Double

Dim wid As Single
Dim Hht As Single

'Dynamic Array of Temperature distribution according to the user i/p
Dim Tmp() As Double

Private Sub Command1_Click()

Dim k, j As Integer
txt11 = ""
txt12 = ""
Text9.Enabled = False

Inputblock    'Gets the input from the user form 1


strMyDataString = ""

jmax = Ly / Dy + 1
kmax = Lz / Dz + 1

qygp = YinQ / Dy + 1
qzgp = ZinQ / Dz + 1


If (Check1.Value = 1) Then ' To enable SOR technique calculations
   Dim sigma, pi As Double
   pi = 22 / 7

   omega = 1.8
```

```
 Else
   omega = 1
End If
Text30.Text = Str(omega)

' To define the orientation of sensors installed on the cooled surface.
If (Option1.Value = True) Then
   YSize = Ws
   ZSize = Ls
Else
   YSize = Ls
   ZSize = Ws
End If
Nygps = YSize / Dy + 1 ' # of Y-dir grid points in a sensor
Nzgps = ZSize / Dz + 1 ' # of Z-dir grid points in a sensor
Nygpg = ygap / Dy - 1  ' # of Y-dir grid points in a Gap
Nzgpg = Zgap / Dz - 1  ' # of Z-dir grid points in a Gap
Nygpb = Ybase / Dy     ' # of Y-dir grid points in a Base
Nzgpb = Zbase / Dz     ' # of Z-dir grid points in a Base

Ytotsen = jmax / Nygps + 1  'Guess value of total sensors in y-dir
Ztotsen = kmax / Nzgps + 1  'Guess value of total sensors in z-dir

ReDim ysentbl(1 To Ytotsen, 1 To 3)
ReDim zsentbl(1 To Ztotsen, 1 To 3)



' Create sensor location table; one for y-dir
Dim temp1, temp2 As Integer
Dim ii As Integer
ysentbl(1, 1) = 1
ysentbl(1, 2) = Nygpb + 1
ysentbl(1, 3) = ysentbl(1, 2) + Nygps - 1
For ii = 2 To Ytotsen
   temp1 = ysentbl(ii - 1, 3) + Nygpg + 1
   temp2 = temp1 + Nygps - 1
   If (temp1 < jmax And temp2 <= jmax) Then
      ysentbl(ii, 1) = ii      ' Sets the Y-index # for the sensor
      ysentbl(ii, 2) = temp1   ' Sets the lower limit of a particular sensor
      ysentbl(ii, 3) = temp2   ' Sets the upper limit of a particular sensor
      Ytotsen = ii
   Else
      GoTo 41
   End If
Next ii
```

```
' Create sensor location table; one for z-dir
41 zsentbl(1, 1) = 1
zsentbl(1, 2) = Nzgpb + 1
zsentbl(1, 3) = zsentbl(1, 2) + Nzgps - 1
For ii = 2 To Ztotsen
   temp1 = zsentbl(ii - 1, 3) + Nzgpg + 1
   temp2 = temp1 + Nzgps - 1
   If (temp1 < kmax And temp2 <= kmax) Then
   zsentbl(ii, 1) = ii      ' Sets the Z-index # for the sensor
   zsentbl(ii, 2) = temp1   ' Sets the lower limit of a particular sensor
   zsentbl(ii, 3) = temp2   ' Sets the upper limit of a particular sensor
   Ztotsen = ii
   Else
      GoTo 51
   End If
Next ii

51  ytop = jmax - ysentbl(Ytotsen, 3)
   ztop = kmax - zsentbl(Ztotsen, 3)


imx = (Lx + Hs) / Dx + 1
Alpha = (Dy * Dz) ^ 2
Beta = (Dx * Dz) ^ 2
Gama = (Dx * Dy) ^ 2
Nue = 2 * (Alpha + Beta + Gama)
intfac = Lx / Dx + 1

ReDim Tmp(1 To imx, 1 To jmax, 1 To kmax) As Double


      initializ   ' Set an initial eduacated guess at liquid helium temp.
      tlevel
'5 Unload Form2

End Sub
Sub Domenlmt()
Dim i As Integer

For i = 2 To nez
   kmin(i) = kmax(i - 1) + 1
   kmax(i) = kmin(i) + kmax(1) - 1
Next i
jmin(1) = 1
jmax(1) = Ly / ney
```

```
For i = 2 To ney
   jmin(i) = jmax(i - 1) + 1
   jmax(i) = jmin(i) + jmax(1) - 1
Next i
tmx = (ToT / Dt) + 1
imx = (Lx / Dx) + 1

End Sub
Sub Inputblock()
Lx = Val(Text1.Text)
Ly = Val(Text2.Text)
Lz = Val(Text3.Text)

Dx = Val(Text5.Text)
Dy = Val(Text6.Text)
Dz = Val(Text7.Text)

KNb = Val(Text16.Text)
Kg10 = Val(Text15.Text)

Ls = Val(Text4.Text)
Ws = Val(Text8.Text)
Hs = Val(Text9.Text)
Zbase = Val(Text12.Text)
Ybase = Val(Text23.Text)
Zgap = Val(Text19.Text)
ygap = Val(Text24.Text)

Epsilon = Val(Text28.Text)

q = Val(Text25.Text)
YinQ = Val(Text26.Text)
ZinQ = Val(Text27.Text)


Hf = Val(Text17.Text)
Tf = Val(Text18.Text)


End Sub
Private Sub tlevel()
Dim i, k, j, tind As Integer
Dim cnt As Integer

itr = 1
Errmx = 1
```

```
While (Errmx > Epsilon)

   xyswpzpge   ' 3D Laplace equation solving scheme.i.e. sweep on
          'xy face with paging in z-direction
cnt = itr / 20
If (itr = cnt * 20) Then
   Text29.Text = Str(itr)
   Text13.Text = Str(Errmx)
   Form1.Refresh
End If

itr = itr + 1
Wend

  Text29.Text = Str(itr)
  Text30.Text = Str(omega)


' Output Format Section of the Program
5   For j = 1 To jmax

      For k = 1 To kmax

         strMyDataString = strMyDataString & Str(Format(Tmp(intfac, j, k),
"##.00000000")) & vbTab

      Next k
   strMyDataString = strMyDataString & vbCr
   Next j

' Calling Output file for the storage of the computed data
pstproc

End Sub

Private Sub initializ()
' This provides temperature initial conditions
Dim i As Integer
Dim j As Integer
Dim k As Integer

' Note!
   ' A RECTANGULAR DOMAIN (INCLUDING THE SENSORS IN IT) IS
'ASSUMED FOR APPLYING UNIFORM INITIAL GUESS VALUEs. BUT THE
'POINTS OUTSIDE THE ACTUAL DOMAIN SHALL NOT BE COMPUTED
   ' IN THE MAIN PROGRAM.
```

```
    For i = 1 To imx
       For j = 1 To jmax
         For k = 1 To kmax
             Tmp(i, j, k) = Tf ' Initial Guess temp equal to fluid temp Tf
         Next k
       Next j
    Next i

End Sub


Public Sub Ysenloc(jk)

Dim ii As Integer
Ysensr = False
For ii = 1 To Ytotsen
    If (jk >= ysentbl(ii, 2) And jk <= ysentbl(ii, 3)) Then
       Ysensr = True
       YsenNUM = ii
       YsLL = ysentbl(ii, 2)
       YsUl = ysentbl(ii, 3)
       GoTo 5
    End If
Next ii

5 End Sub
Public Sub Zsenloc(jk)

Dim ii As Integer
Zsensr = False
For ii = 1 To Ztotsen
    If (jk >= zsentbl(ii, 2) And jk <= zsentbl(ii, 3)) Then
       Zsensr = True
       ZsenNUM = ii
       ZsLL = zsentbl(ii, 2)
       ZsUL = zsentbl(ii, 3)
       GoTo 5
    End If
Next ii

5 End Sub
Public Sub xyswpzpge()

Dim i, j, k, SC As Integer
Dim AMn, AMx, BMn, BMx, CMn, CMx, tempo As Double
```

```
Dim kk As Double
Dim constt, const1, const2, const3, const2y, const3z As Double
Errmx = 0

flag = False
 For k = 1 To kmax
  Call Zsenloc(k)
  For j = 1 To jmax
    Call Ysenloc(j)
    If (Ysensr = True And Zsensr = True) Then
      flag = True
    Else
      flag = False
    End If

    If (flag = False) Then
      imax = Lx / Dx + 1
      kk = KNb
    Else
      imax = imx
      kk = Kg10
    End If

    constt = 6 * Hf / 11 / kk
    const1 = 1 + constt * Dx
    const2 = 1 + constt * Dy
    const2y = 1 - constt * Dy
    const3 = 1 + constt * Dz
    const3z = 1 - constt * Dz



    For i = 1 To imax

     'IMPLEMENTATION OF X-DIRECTION BOUNDARY CONDITIONS

      ' Inside the computational domain when not on any of the boundary
      If (i <> 1 And i <> intfac And i <> imax) Then
        AMn = Tmp(i - 1, j, k)

      ' On the Heated surface excluding point heating
      ElseIf (i = 1 And (j <> qygp Or k <> qzgp)) Then
        AMn = Tmp(i + 1, j, k) '

      ' On the Heated surface at the point of heating
```

```
        ElseIf (i = 1 And j = qygp And k = qzgp) Then AMn = 2 * Dx * q / KNb + Tmp(i
+ 1, j, k)

        ' At the interface of Niobium and the Sensor
        ElseIf (imax <> intfac And i = intfac) Then AMn = 2 * KNb / (KNb + Kg10) *
Tmp(i - 1, j, k)

        ' At the cooled surface
        ElseIf (i = imax) Then AMn = 1 / const1 * (2 / 11 * Tmp(i - 3, j, k) - 9 / 11 *
Tmp(i - 2, j, k))

        End If

        ' Inside the computational domain when not on any of the boundary
        If (i < imax And i <> intfac) Then AMx = Tmp(i + 1, j, k)

        ' At the cooled surface
        If (i = imax) Then AMx = 1 / const1 * (18 / 11 * Tmp(i - 1, j, k) + constt * Dx *
Tf)

        ' At the interface of Niobium and the Sensor
        If (flag = True And i = intfac) Then AMx = 2 * Kg10 / (KNb + Kg10) * Tmp(i +
1, j, k)

    ' Implementation of Y and Z Direction boundary conditions
        If (i <= intfac) Then     ' when i is in Niobium computational domain
          If (j = 1) Then
            BMn = Tmp(i, j + 1, k)
            BMx = Tmp(i, j + 1, k)

          ElseIf (j = jmax) Then
            BMn = Tmp(i, j - 1, k)
            BMx = Tmp(i, j - 1, k)
          Else
            BMn = Tmp(i, j - 1, k)
            BMx = Tmp(i, j + 1, k)

          End If

          If (k = 1) Then
            CMn = Tmp(i, j, k + 1)
            CMx = Tmp(i, j, k + 1)

          ElseIf (k = kmax) Then
            CMn = Tmp(i, j, k - 1)
            CMx = Tmp(i, j, k - 1)
```

```
    Else
        CMn = Tmp(i, j, k - 1)
        CMx = Tmp(i, j, k + 1)
    End If
Else            ' when i is in sensor computational domain
    ' For Y-Direction Boundary Conditions
    If (j <> YsLL And j <> YsUl And j <> 1 And j <> jmax) Then
        BMn = Tmp(i, j - 1, k)
        BMx = Tmp(i, j + 1, k)
    ElseIf (j = 1) Then
        BMn = Tmp(i, j + 1, k)
        BMx = Tmp(i, j + 1, k)
    ElseIf (j = YsLL And j <> 1) Then
        BMn = 1 / const2y * (18 / 11 * Tmp(i, j + 1, k) - 9 / 11 * Tmp(i, j + 2, k))
        BMx = 1 / const2y * (2 / 11 * Tmp(i, j + 3, k) - constt * Dy * Tf)
    ElseIf (j = YsUl And j <> jmax) Then
        BMn = 1 / const2 * (2 / 11 * Tmp(i, j - 3, k) - 9 / 11 * Tmp(i, j - 2, k))
        BMx = 1 / const2 * (18 / 11 * Tmp(i, j - 1, k) + constt * Dy * Tf)
    ElseIf (j = jmax) Then
        BMn = Tmp(i, j - 1, k)
        BMx = Tmp(i, j - 1, k)
    End If

    ' Similarly for conditions in Z-Direction
    If (k <> ZsLL And k <> ZsUL And k <> 1 And k <> kmax) Then
        CMn = Tmp(i, j, k - 1)
        CMx = Tmp(i, j, k + 1)
    ElseIf (k = 1) Then
        CMn = Tmp(i, j, k + 1)
        CMx = Tmp(i, j, k + 1)
    ElseIf (k = ZsLL And k <> 1) Then
        CMn = 1 / const3z * (18 / 11 * Tmp(i, j, k + 1) - 9 / 11 * Tmp(i, j, k + 2))
        CMx = 1 / const3z * (2 / 11 * Tmp(i, j, k + 3) - constt * Dz * Tf)
    ElseIf (k = ZsUL And k <> kmax) Then
        CMn = 1 / const3 * (2 / 11 * Tmp(i, j, k - 3) - 9 / 11 * Tmp(i, j, k - 2))
        CMx = 1 / const3 * (18 / 11 * Tmp(i, j, k - 1) + constt * Dz * Tf)
    ElseIf (k = kmax) Then
        CMn = Tmp(i, j, k - 1)
        CMx = Tmp(i, j, k - 1)
    End If

End If


tempo = Tmp(i, j, k)
```

```
        Tmp(i, j, k) = Tmp(i, j, k) + omega * ((1 / Nue * (Alpha * (AMn + AMx) + Beta *
(BMn + BMx) + Gama * (CMn + CMx))) - Tmp(i, j, k))

        ' Monitor the Absolute Error at each grid point
        Error = Abs(Tmp(i, j, k) - tempo)

        ' Trap the maximum error in each itration
        If (Error > Errmx) Then Errmx = Error


     Next i
    Next j
   Next k

  End Sub

Private Sub Command2_Click()
End
End Sub

Private Sub Form_Load()
Text9.Enabled = False

End Sub

Sub pstproc()
 'this program :-
  '1. checks to see if there is a folder on C drive called "C:\DataResult\"
  '2. If finds it then Ok, if not then creates a folder.
  '3. Then checks to see if there is a file named C:\DataResult\MyDataFile-1.xls
  '4. If found then cheks to see if there is a file named C:\DataResult\MyDataFile-2.xls
  '5. Keeps trying till it finds a name that is not in use in that folder.
  '6. Creates a file at the location found in step 5.
  '7. Everytime  run this program it will create a new file.


  Dim objFSO As New Scripting.FileSystemObject
  Dim objTextStream As Scripting.TextStream

  Dim strCompletePath As String
  Dim strFolderName As String
  Dim strFileName As String
  Dim strFileExtension As String


  strFolderName = "C:\DataResult\"
```

```
  strFileName = "MyDataFile"
  strFileExtension = ".xls"

  Dim blnFileNameFound As Boolean
  Dim intFileNameCount As Integer

  strCompletePath = strFolderName & strFileName

   ' first Check to see if the folder exists if it doesnt then create one
   If objFSO.FolderExists(strFolderName) = False Then
         'folder doesnt exist so create one
         objFSO.CreateFolder strFolderName
   End If

   ' check to see if folder was created
      If objFSO.FolderExists(strFolderName) = False Then
         'folder doesnt exist so create one
         MsgBox "Failed to create a folder at : " & strFolderName
         GoTo DestroyObjects
   End If

   blnFileNameFound = False
   Do While blnFileNameFound = False    ' Means keep looping till a new file name is
'decided
      intFileNameCount = intFileNameCount + 1
      strCompletePath = strFolderName & strFileName & "-" & intFileNameCount &
strFileExtension
      If objFSO.FileExists(strCompletePath) = False Then
         ' File name is unique exit
         blnFileNameFound = True
      End If
   Loop


   If Len(strMyDataString) > 0 Then
      Set objTextStream = objFSO.OpenTextFile(strCompletePath, ForWriting, True,
TristateUseDefault)
      objTextStream.Write strMyDataString
      objTextStream.Close
   Else
      MsgBox "There was no data provided so file was not created"
   End If

   If objFSO.FileExists(strCompletePath) = True Then
      MsgBox "Data file was successfully created at " & strCompletePath
   Else
```

```
    MsgBox "Data file was NOT created"
  End If

DestroyObjects:
' Set all objects to nothing otherwise they will stay in the memory
 Set objFSO = Nothing
 Set objTextStream = Nothing
End Sub
```

## 5.2 Properties Of Liquid Helium

### 5.2.1 Background

Janssen first discovered traces of helium during the solar eclipse of 1868 in the solar spectrum of which he detected a new line. Kaerlingh Onnes in his laboratory first achieved liquification of helium in 1908 by using liquid hydrogen pre-cooling in a Joule-Thomson liquefier.

### 5.2.2 Isotopes of Helium

Helium has two isotopes, known as helium-3 and helium-4. The helium-4 is a more common isotope, which consists of two electrons surrounding a nucleus of two neutrons and two protons. The helium-3 atom consists of two electrons surrounding a nucleus of two protons plus one neutron.

### 5.2.3 Liquid Helium

As described above, helium-4 is the most common of the two isotopes. Ordinary helium gas consists of about $1.3\times10^{-4}$ percent helium-3, so usually when reference is made to liquid helium or helium, generally helium-4 is being referred to. It has a molecular weight 4.0026.

### 5.2.4 General Properties of Helium

Liquid helium-4 is odorless and colorless and sometimes difficult to see in a container. Table 4 lists some of its properties [10].

| | |
|---|---|
| Boiling point temperature | 4.224 K |
| Density at normal boiling point<br>Liquid<br>Vapor | <br>124.96 kg/m$^3$ or 0.03122 $mol/cm^3$<br>16.89 kg/m$^3$ or 0.00422 $mol/cm^3$ |
| Heat of vaporization at normal boiling point | 10.73 kJ/kg |
| Solidification point at normal atmospheric pressure | Doesn't exist even if temperature is reduced to absolute zero |
| Index of refraction $n_r$ | 1.02 |

Table 4 General properties of liquid helium

5.2.5 Unique Properties of Liquid Helium

Liquid helium has number of unique properties, which are not present in many other liquids. One of the first properties of liquid helium that attracted great attention is the absence of solid-liquid-vapor triple point. The most amazing properties, however, are those shown by liquid helium at temperatures below 2.17 k. As the liquid is cooled below this temperature, instead of solidifying, it changes to a new liquid phase hence marking another distinct transitional line on the phase diagram. This transitional line separates the two phases of liquid helium. Liquid helium above this transitional line is known as helium-I and liquid helium below this transitional line is known as helium-II. Properties of helium-II are remarkable as it does not obey normal laws. Helium-II expands on cooling: its conductivity for heat is enormous and is as high as 86,500 W/m K – much higher than that of pure copper at room temperature [1]. In fact, measurement of true values of thermal conductivity below the transition point, known as lambda point, is very hard to make. As an estimate, k for He II below the transition point is about 80,000 W/m-K between 1.4 and 1.75 K and it might go as high as 340,000 W/m-K at 1.92 K. These values are the highest conductivities known of copper, silver, and diamond [11].

## 5.3 Temperature Measurements

### 5.3.1 Defining Temperature Measurement [5]

Temperature is not a directly measurable quantity, but rather inferred from other measurements, which can be made directly. All measurements have an associated uncertainty, u, which depends on the statistical nature of the measurement. The choice of resolution, precision or, accuracy as the important statistical feature of the measurement can be important. Good resolution is easiest to achieve and good accuracy is hardest to achieve. Selecting an inappropriate statistical measure either adds cost to or decreases the value of a measurement. As an example, resolution is the most important statistical measure if small temperature changes must be measured, but the absolute temperature either is not important or can be measured independently. Precision is most important when successive measurements under identical conditions must return the same value, but the true value of the quantity is not required. An example might be a temperature control system, which must run successive samples through identical temperature cycles, but the actual temperatures are less important than the repeatability of the cycles. Accuracy is most important when absolute temperature must be known.

It is always true that the accuracy is worse than the precision, and precision is worse than the resolution of a measurement.

No temperature sensor operates by itself. The expected resolution, precision and accuracy of a temperature measurement depend not only on the properties of the temperature sensor, but also on the measurement system and the sensor's thermal environment.

5.3.2 Uncertainty Conversions Using Dimensionless Sensitivities

A sensor produces some output signal such as a voltage, frequency, resistance or capacitance, which is measured by the instrumentation.

Uncertainties in the measured quantity are not in units of temperature and must be converted. In the case of a temperature sensor with an output Resistance R, the temperature $u_T$ uncertainty is related to the resistance uncertainty $u_R$ by the dimensionless formula

$$\frac{u_T}{T} = \frac{u_R/R}{(T/R)(dR/dT)} \equiv \frac{u_R/R}{S_T} \qquad 5.1$$

Where $S_T = (T/R)(dR/dT)$ is defined as the dimensionless temperature sensitivity. The dimensionless sensitivity is also equal to d(log R)/d(log T), the slope of the resistance verses temperature curve on a log-log plot. There are advantages to this form of the equation. First, the dependence of the resolution upon the excitation is now explicit rather than implicit in the sensitivity. Second, the dimensionless nature of equation 5.1 allows its application to thermometers based on other temperature dependant properties (capacitance, voltage, or pressure) by replacing R with C, V, or P as appropriate. This allows for easier comparison of calculation of resolutions based on different temperature-dependent properties.

A dimensionless sensitivity in the 0.1 to 10 range is usually best for property measurements over a wide range, although other factors such as physical size or sensitivity to environmental conditions can be much more important. A large dimensionless sensitivity allows good relative temperature resolution, but the temperature range becomes limited if the value of the property measured becomes too large or small to be determined accurately.

### 5.3.3 Resolution

Resolution is given the symbol r and has the same units as the quantity measured. The smallest distinguishable change in a temperature measurement is termed the temperature resolution, $r_T$. The temperature resolution is often determined by some limiting factor in the measurement system. The resolution of a digital system is typically determined by the smallest unit change, which can be displayed and is usually a fixed value for a given range. In the simple case of a temperature readout displaying three digits to the right of the decimal, the temperature resolution is 0.001 times the temperature unit (e.g. K or $^oC$ ).

As an example, consider an instrumentation system consisting of an Ohmmeter with a 5-digit display capable of displaying 0 to 99999 counts. If the smallest range is 0-10 $m\Omega$, then the best resistance resolution, $r_R$ is 9.9999 $m\Omega$/99999=0.1 $\mu\Omega$. A resistance 10 $m\Omega$ or larger must be read on another scale with poorer resolution. The resulting temperature resolution can be calculated using

$$r_T = \frac{r_R}{(dR/dT)} \qquad 5.2$$

where $r_T$ is the temperature resolution, $r_R$ is the resistance resolution, and dR/dT is the sensitivity of the sensor. Note that the sensitivity dR/dT is a function of both temperature and excitation while $u_R$ is fixed by the instrument design for a given range. The relative resolution is defined as the temperature resolution divided by the absolute temperature and can be calculated using dimensionless quantities as

$$\frac{r_T}{T} = \frac{(r_R/R)}{(T/R)(dR/dT)} = \frac{(r_R/R)}{S_T} \qquad 5.3$$

Hence, in general, the sensor with the best resolution will depend on the measurement system and considerations other than the resolution can be very important in selection of a sensor.

5.3.4 Precision And Accuracy

The probable precision or accuracy of a temperature measurement is never better than the resolution of and typically depends on several additional factors. Estimating the precision or accuracy of a measurement involves the following steps

- Identify the relevant sources of measurement uncertainty.
- Change the units of all uncertainties to temperature, and
- Combine all of the uncertainties using the root sum of squares method as described later.

Examples of source of measurement uncertainties affecting the accuracy, but not the precision of a measurement include offset voltages and calibration uncertainties.

5.3.5 Sources Of Measurement Uncertainty

The following sections discuss specific sources of temperature measurement uncertainty and how to estimate their magnitudes.

(a) Instrumentation Measurement Uncertainty. The manufacturer normally specifies the accuracy of the instrument measuring the output of a temperature sensor. The accuracy of a digital meter is usually specified as a percentage of reading plus a number of counts of the least significant digit. The percent accuracy is calculated as a function of the actual reading, not full scale as done for analog meters. For example, a digital accuracy specification of $\pm$(0.05%+1 count) for 4-1/2 digit meter reading 3.000 m$\Omega$ on a 20 m$\Omega$ range equals a resistance uncertainty $u_R$ of $\pm$(0.0015+0.001) m$\Omega$ = $\pm$2.5 $\mu\Omega$. Equation 1 is again used to translate to temperature uncertainty.

(b) Sensor Self-Heating. Any difference between the temperature of the sensor and environment the sensor is intended to measure produces a temperature measurement error or uncertainty. Dissipation of power in the temperature sensor will cause its temperature to rise above that of the surrounding environment. Power dissipation in the sensor is also necessary to make a temperature measurement. Minimization of the temperature measurement uncertainty thus requires balancing the uncertainties due to self-heating and output signal measurement. Attempting to correct for 'self heating' errors by calculation or extrapolation is not considered good practice. An estimate of the 'self heating' errors should be included in the total uncertainty calculation instead.

(c) Thermal (Johnson) Noise Thermal energy produces random motions of the charged particles within a body, giving rise to electrical noise. The minimum root mean square (rms) noise power available is given by $P_n = 4kT\Delta f_n$, where k is the Boltzmann constant and $\Delta f_n$ is the noise bandwidth. Peak-to-peak noise is approximately five times greater than the rms noise. Metallic resistors approach this fundamental minimum, but other materials produce somewhat greater thermal noise. The noise bandwidth is not necessarily the same as the signal bandwidth, but is approximately equal to the smallest of the following [Low Level Measurements, Keithley Instruments, Inc., Cleveland, Ohio, USA (1993).]

- $\pi/2$ times the upper 3 db frequency limit of the analog DC measuring circuitry, given as approximately 1/(4 $R_{eff}C_{in}$) where $R_{eff}$ is the effective resistance across the measuring instrument (including the instrument's input impedance in parallel with the sensor resistance and wiring) and $C_{in}$ is the total capacitance shunting the input;
- $0.55/t_r$ where $t_r$ is the instrument's 10%-90% rise time;
- 1 Hz if an analog panel meter is used for readout; or
- One half the conversion rate (readings per second) of an integrating digital voltmeter.

(d) Thermoelectric And Zero Offset Voltages Voltages develop in electrical conductors with temperature gradients when no current is allowed to flow (Seeback effect). Thermoelectric voltages appear when dissimilar metals are joined and joints are held at different temperatures. Typical thermoelectric voltages in cryogenic measurement systems are on the order of microvolts.

A zero offset is the signal value measured with no input to the measuring instrument. The zero offset can drift with time or temperature and is usually included in the instrument specifications. Thermoelectric voltages and zero offsets can be eliminated from voltage measurements on ohmic resistors by reversal of the excitation current and use of the formula:

$$V = (V_+ - V_-)/2$$

Where $V_+$ and $V_-$ are the voltages with respectively positive and negative excitation currents. Alternating current (AC) excitation can also be used with ohmic sensors to eliminate zero offsets. The sum of the thermoelectric voltages and zero offset can be calculated as

$$V_o = (V_+ + V_-)/2$$

Note that the resolution of $V_o$ is practically limited by the resolution of the measured system. The value of $V_o$ can be expected to vary little in a static system, but may change during a thermal transient under study. The value of $V_o$ should be rechecked as often as practical. The offset voltage $V_o$ is best measured by reversing the current through a resistor. Measurement of $V_o$ with zero excitation current is also possible, but large resistances can produce excessive time constants for discharge of any capacitances in the circuit, requiring long waiting times before $V_o$ can be measured accurately.

(e) Environmental Effects Temperature sensors can be affected by changes in the environment. Examples include magnetic fields, ionizing radiation, or changes in the pressure, humidity, or chemistry of environment.

(f) Ground Loops. Improper grounding of instruments or grounding at multiple points can allow current flows which result in small voltage offsets. One common problem is the grounding of cable shields at both ends. The current flow through ground loops is not necessarily constant, resulting in a fluctuating voltage.

(g) Electromagnetic Noise Electromagnetic pickup is a source of additional noise. Alternating current noise is a serious problem in sensors with nonlinear current-voltage characteristics. Measurement of the AC noise across the terminals of the reading instrument can give a quick indication of the magnitude of this noise source (thermal noise will be included in this measurement). Twisting wire pairs, using coaxial cables, adding shielding, or shortening the wires can reduce electromagnetic pickup.

5.3.6 Calibration Uncertainty

Commercially calibrated sensors should have calibrations traceable to international standards. The calibration uncertainty typically increases by a factor of 3 to 10 between successive devices used to transfer a calibration. An algorithm for selecting the number and spacing of calibration points is given by Nara, et al [6].

5.3.7 Combining Measurement Uncertainties

The expected uncertainty of a measurement is expressed in statistical terms. As stated in the guide to the expression of uncertainty in measurement: [7].

"The exact values of the contributions to the error of the measurement arising from the dispersion of the observations, the unavoidable imperfect nature of the corrections, and incomplete knowledge are unknown and unknowable, whereas the uncertainties associated with these random and systematic effects can be evaluated........the uncertainty of a result of a measurement is not necessarily an indication of the likelihood that the measurement result is near the value of the measurement; it is simply an estimate of the likelihood of nearness to the best value that is consistent with presently available knowledge."

The uncertainty, u, has the same units as the quantity measured. The combined uncertainty $u_c$ arising from several independent uncertainty sources discussed above can be estimated by assuming a statistical distribution of uncertainties, in which case the uncertainties are summed in quadrature according to

$$u_c = \sqrt{u_1^2 + u_2^2 + \ldots + u_i^2 + \ldots + u_n^2} \qquad 5.4$$

Both random and systematic uncertainties are treated in the same way. The justification for this practice is given in Annex E of Reference [7]. Note that both sides of equation 4.4 can be divided by the measurement quantity to express the measurement uncertainty in relative terms. Finding statistical data suitable for addition by quadrature can be a problem; instrument and sensor specification sometimes give maximum or typical values for uncertainties. Two approaches may be taken to dealing with maximum uncertainty specifications. The conservative approach is to use the specification limit value in the combined uncertainty calculation. The less conservative approach is to assume a statistical distribution within the specification limits and assume the limit is roughly three standard deviations, in which case one third of the specification limit is used in uncertainty calculations. Practical recommendations and procedures for problems related to the estimation of measurement uncertainties are discussed in greater detail by Rabinovich [8].

## 5.4 Super-Conductivity

Super-conductivity was first observed by Kamerlingh Onnes in 1911. It is a state when electrical resistivity of a material suddenly drops to zero at a temperature known as the critical temperature. This state is found in many materials and it occurs when the material is sufficiently cooled, often to temperatures in the liquid helium range.

In the simple free electron picture for the behavior of a metal, electrons in the outer shells of atoms in a metal are easily detached from the core and wander away from the parent ions that define the solid lattice and are responsible for the excellent electrical and thermal conductivity of metals.

At temperatures above the critical temperature, these atoms are not organized and remain disordered. However, the electrons are ordered at temperatures below the transition temperature. Thus the transformation from the normal state to the super-conducting state may be considered to be a phase change involving the electronic state while not affecting the crystal structure of the material [12].

It has been stated that the super-conducting state is an ordered state. Super-conductivity can be considered as arising from the coupling between pairs of electrons and vibrating atoms. In the super-conducting state, pairs of electrons develop an attractive interaction by simultaneously interacting with vibrating atoms. When one electron of the electron pair is scattered, the other responds so that there is no net effect on the motion of the pair. If the thermal energy of the atom is sufficient it will disrupt the coupling. Thus super-conductivity is only observed at very low temperatures where the thermal energy of the atom will be insufficient to destroy the electron pair coupling.

# REFERENCES


1. H. Padamsee, "Calculations For Breakdown Induced by Large Defects in Superconducting niobium cavities", IEEE transactions on magnetics, vol-19, No.3, 1322(1983)
2. K.R. Krafft, "An investigation of Thermal Transport in Superconducting Cavities Made of High Thermal Conductivity niobium", IEEE transactions on magnetics, vol. Mag-19 pg 1326
3. H.P. Kramer, "Heat Transfer to Forced Flow Helium II", Proceedings of 12$^{th}$ ICEC Southampton UK 1988, page 299.
4. R. Romijn, W. Weingarten and H. Piel, "Calibration of the Scanning Thermometer Resistor System for a Superconducting Accelerating Cavity", IEEE transactions on magnetics, vol. Mag-19, pg 1318
5. "Temperature Measurement and Control" Lake Shore Cryotronics, Inc.
6. . k.Nara, H.kato and M.Okaji, "Derivation of optimized calibration procedures for practical thermometers", Cryogenics 35 (1995) 291-295
7. "ISO Guide to the Expression of Uncertainty in Measurement", first edition, ISO/TAG 4/WG 3, International Organization for Standardization, Geneva, Switzerland (1992)
8. S. Rabinovich, "Measurement Errors", American Inst. of Phs.(1993)
9. Hasan Padamsee, Jens Knobloch, and Tom Hays "RF Superconductivity For Accelerators", John Wiley & Sons, INC, 1998.
10. Timmerhaus D. and Thomas M.Flynn, Cryogenic Process Engineering.
11. Lienhard H.John and Chap. 6 by Roger Eichhorn, "A heat transfer textbook"

12. Irving Granet, "Modern Material Science", page 408. Reston Publishing Company Inc. A PRENTICE-HALL COMPANY.

13. Frank P. Incropera, David P. DeWitt "Introduction to Heat Transfer" John Wiley & Sons, 1990.

14. Brice Carnahan and James O. Wilkes, "Numerical Methods, Optimization Techniques and Process Simulation For Engineers"; p.279 (1967)

15. J. Beck, R. McMasters, A Haji-Sheikh, "COND3D, Computer Code for Computing Exact Solutions for Transient Heat Conduction in Three-Dimensional Parallelepipeds", Under Contact to Sandia National Laboratories, Albuquerque, NM, 2002.

16. D. Tullock and E. Montalbano, "Kokopelli 96.2 Finite Element Program", Los Alamos National Laboratory, Los Alamos, NM, 1996.